12-2004

Carbon Nanotube Based Chemical and Biological Sensors

Srikanth Singamaneni

CARBON NANOTUBE BASED CHEMICAL AND BIOLOGICAL SENSORS

by

Srikanth Singamaneni

A Thesis
Submitted to the
Faculty of The Graduate College
in partial fulfillment of the
requirements for the degree of
Master of Science in Engineering (Electrical)
Department of Electrical and Computer Engineering

Western Michigan University
Kalamazoo, Michigan
December 2004

ACKNOWLEDGEMENTS

Firstly, I would like to acknowledge many great researchers who have been working in the field of carbon nanotubes. S. Iijima for his groundbreaking discovery of MWNT, C. Dekker for his valuable contribution in understanding the electronic properties of CNT, H. Dai for his pioneering efforts in CNT based chemical sensors, R.E. Smalley group for their wonderful contributions to the field of fullerene science and many others without whom this thesis could have never existed.

I would like to express my earnest gratitude to my advisor Dr. Massood Z. Atashbar, for his continuous support in all aspects of the project. He has been a constant source of dedication and the driving force behind the successful completion of the project. I would like to thank Dr. Bruce Bejcek for his valuable discussions and also providing me access to his laboratory facilities. I am grateful to Dr. John Gesink for kindly accepting to be on my thesis committee. I would like to thank Dr. Valery Bliznyuk for providing me the access to his laboratory. I would like acknowledge the financial support from the Department of Defense under the contract number W81XWH-04-10250.

I always had the habit of sharing my experiences during various experiments. Special thanks are due to Ms. Sridevi Krishnamurthy for patiently entertaining the lengthy discussions of my experiments. I would like to thank Mr. Aditya Vijh and Mr. Shakil Hossein for the help and technical support they provided in conducting the

experiments. Also, I would like to acknowledge Mr. Giridhar Vejendla and Ms. Deepthi Karlapudi for being with me throughout my Masters and bearing with all my emotions. I would like to thank Amma (Mom), Nanna (Dad), Annayya (Brother) and my friend Mr. Somnath Metla for showing me the wonderful colors of life. Finally, I would like to dedicate the thesis to "SCIENCE" which I believe is the most wonderful entity in the universe.

Srikanth Singamaneni

CARBON NANOTUBE BASED CHEMICAL AND BIOLOGICAL SENSORS

Srikanth Singamaneni, M.S.E.

Western Michigan University, 2004

Carbon nanotubes are among those wonderful molecules man has discovered by chance. Carbon nanotubes are sheets of graphite rolled up to form seamless cylinders. Their outstanding electrical, mechanical and thermal properties form the inspiration behind this work. This work investigates the possible application of carbon nanotubes as biological sensors for the detection of various biomolecules like Streptavidin and Mouse monoclonal Immunoglobulin-G. Electrical conductance changes of Carbon nanotubes for exposure to alcohol vapors were studied. This thesis demonstrates that these quantum wires can form highly sensitive biological and chemical sensors at molecular level. Although the main focus of the research was chemical and biological sensor applications of carbon nanotubes some other interesting studies related to the basic science of the carbon nanotubes could not be overlooked. Comparative studies of the Raman spectra of carbon nanotubes and Highly Oriented Pyrolytic Graphite at elevated temperatures have been conducted. The decrease in the intensity of the signal and also the change in the Raman shift of the 'G' band are discussed. The thesis also reveals some interesting facts about surfactant treatment of carbon nanotubes. The improved dissolution of carbon nanotubes by surfactant treatment is elucidated. This is a significant step results in the improvement of the biological sensing application of carbon nanotubes.

TABLE OF CONTENTS

Table of Contents-Continued

LIST OF TABLES

LIST OF FIGURES

List of Figures-continued

1. INTRODUCTION

In the December of 1959, at the Annual meeting of the American Physical Society at the California Institute of Technology, Richard Feynman delivered a visionary talk, which revolutionized the thinking of modern engineers. The idea of the entire talk can be summarized into a single sentence "*There's Plenty of Room at the Bottom*". He proposed a completely new facet of miniaturization namely the "bottom up" approach. Although there was no experimental backup for his ideas that day, he proposed several ideas of nanoscience and technology obeying the basic physics and fundamental laws of chemistry. This was the starting point of the great revolution of "Nanotechnology", which is influencing and going to influence human civilization in the decades to come.

Although there are many definitions for the term Nanotechnology a simple and accurate one by Meyya Meyyappan is "*Nanotechnology is the creation of functional materials, devices and systems through control of matter on the nanometer length scale (1-100 nanometers), and exploitation of novel phenomena and properties (physical, chemical, biological, mechanical, electrical...) at that length scale.*"

Work based on Nanotechnology can be classified into two types. Firstly, the study of basic physics involved behind behavior of matter at nanoscale in order to establish the set of rules of the game. Secondly, the application oriented experimental work in order to create functional systems and subsystems at nanoscale. Both the areas of work are interdisciplinary and demand wide knowledge of various fields of science.

In order to create functional systems at the nanoscale, novel materials with useful properties (structural, electrical, mechanical, thermal...) are highly desirable. Carbon

Nanotubes (CNTs) fall into those set of novel materials with extremely useful and unique properties [1,2,3]. The discovery of carbon nanotube [4] is a serendipity, which turned out to be a boon to the field of nanoscience. They were discovered by a Japanese scientist Sumio Iijima of NEC Corporation Japan in 1991. CNTs are of two types: single walled and multi walled carbon nanotubes. Although they can be imagined as single sheets of graphene rolled into cylinders, the properties of these one-dimensional quantum wires [5] are exceptional and very different from other forms of carbon.

This work basically involves two different areas of study of these molecular wires. The first part involves the characterization of these novel materials by Raman spectrum in which the temperature dependence of the spectrum is explored. The second part involves the investigation of the possible application of these quantum wires as biological and chemical sensors. Although the above mentioned studies were the focus of the work, we came across several other interesting phenomena related to carbon nanotubes during the course of these studies. Since they were closely related to the main stream of the work they have been discussed in the appropriate areas.

The organization of the thesis is as follows. Following the introduction, chapter 2 is a brief discussion on the background and significance of the work to the current state of research. This involves the state of problem of carbon nanotube based naosensors and systems and a solution approach. In chapter 3, various characterization tools used in the work have been introduced to make the understanding of the later parts of the thesis easier. The major characterization tools involve Atomic Force Microscope, Raman spectrometer, and Quartz Crystal Microbalance. Chapter 4 explains the structure, preparation and properties of carbon nanotube. The physical structure of CNT starting

from graphite sheet is discussed. Although there are a number of methods for the preparation of CNT, the most general and frequently employed techniques are discussed. Electrical, mechanical and thermal properties of CNTs are described. Chapter 5 involves the purification details of CNTs. The CNTs used in the research were purchased and had high percentage of catalyst impurity. A simple yet efficient way to obtain solution of highly purified CNT is discussed. This chapter also includes characterization of purified CNT. This involves the AFM imaging, Raman spectroscopy and electrical characterization. Chapter 6 presents the temperature dependence of Raman spectrum of CNTs. The decrease in the intensity and the downward shift of the 'G' band are discussed. Chapter 7 presents the biosensing applications of CNT. The conductance based sensor based on CNT which exhibited a decrease electrical conductance on the non-covalant binding of the biomolecule and a quantitative measurement of mass of the biomolecule bound using QCM are discussed. Chapter 7 also discusses the CNT electrical sensor response to alcohol vapors. In Chapter 8 various functionalization techniques to improve the solubility of CNT in aqueous solutions and to improve the selectivity of CNT based biosensors is presented. Chapter 9 is the conclusions drawn from the work asserting CNT as a material of the future. This chapter also involves suggestions and guidelines for future work.

1.1. References

[1] J. Tersoff, and R. S. Ruoff, Physics Review Letters, vol. 73, p. 676 (1994).

[2] D. A. Walters, L. M. Ericson, M. J. Casavant, J. Liu, D. T. Colbert, K. L. Smith, and R. E. Smalley, Applied Physics Letters, vol. 74, p. 3803 (1999).

[3] C. T. White, and T. N. Todorov, Nature, vol. 393, p. 240 (1998).

[4] S. Iijima, Nature, vol. 354, p. 56 (1991).

[5] S. J. Tans, M. H. Devoret, H. Dai, A. Thess, R. E. Smalley, L. J. Geerligs, and C. Dekker, Nature, vol. 386, p. 474 (1997).

2. BACKGROUND AND SIGNIFICANCE

Carbon, an element of prehistoric discovery, is widely distributed in nature. It is found in abundance in the sun, stars, comets, and atmospheres of most planets. For centuries, it was believed that the element carbon existed in only two different forms, soft, conductive graphite and hard, transparent, insulating diamond. However, this was proven to be wrong with the discovery of Buckminster fullerene molecule [1] (named after the engineer and architect Richard Buckminster Fuller as the molecules resemble the architecture of his geodesic domes) in 1985 by a group headed by R.E. Smalley from Rice University, which received Nobel Prize in chemistry in 1997. This discovery led to a new branch of organic chemistry called fullerene chemistry. Buckminster fullerene (also known as C_{60}) molecule is composed of hexagons and pentagons of carbon, joined together to form a perfect spherical shape resembling a soccer ball. Soon after this discovery, other molecules like, C_{70}, of the family followed. But C_{60} being most symmetrical of all was also the most stable. The buckyballs behaved very much like electron deficient alkenes and readily react with electron rich species [2].

This new branch of chemistry opened up new horizons in the field of nanoscience and technology. There were many predictions from the chemists all around the world about the possible existence of much more interesting and novel fullerene which is $C_{1,000,000}$. Luck always favors a prepared mind and this time it was Sumio Iijima of NEC Corporation Japan. In his attempt to study carbon fibers formed by arc discharge he ended up discovering the dream molecules "Carbon Nanotubes". He observed from the TEM images that the new molecules were seamless cylinders arranged in a concentric fashion [3]. The intertube distance was exactly equal to inter-plane distance in graphite.

The X-ray diffraction experiments proved that they had carbon atoms in hexagonal fashion. Two years after that, he discovered that smallest manmade tubes with a diameter of nearly 1nm the "Single Walled Carbon Nanotubes". But the real break through came with the discovery of laser ablation technique by R. E. Smalley group for the large-scale synthesis of single wall carbon nanotubes [3]. This discovery has fascinated the scientific community and ever since a lot of research on this buckytubes was carried out. Many properties of this new material have been explored by different groups through out the world and some of them are still points of debate. The transport properties of CNT, most of which were discovered by group headed by Cees Dekker of Delft University (Netherlands), are most promising making them ideal one-dimensional quantum wires for interconnects and also active devices for future molecular electronics [4]. In terms of the mechanical properties nanotubes, are believed to be the strongest and most resilient materials known to exist [5].

Although most of the properties of CNT are discovered, there are still some challenges before the scientific community before utopia of molecular technology is achieved. CNT properties are strongly dependent on the structure of the tube and any known method of fabrication yields nanotubes of a widely varying structure. In order to use these nanotubes in molecular electronics or any other specific applications like molecular sensors, it is essential that the tubes are separated. Also, it is not feasible to pick and place these tubes at desired locations (like between two electrodes possibly drain and source of transistor) in a large-scale production of the molecular devices [6]. Therefore, some kinds of techniques are needed to probably grow the nanotubes with desired properties in desired places in a single chemical process or to somehow self assemble the tubes which will

allow a large scale production of nanotube based devices. Besides these there are some other challenges like how to use these molecular wires as highly sensitive sensors at nanoscale. There are significant advantages for nanosensors over the conventional sensors like lowering the power consumption, the miniaturizing the size space occupied and so on. These factors are of high importance in the sensors related to space research and air craft applications where light weight and highly accurate sensors are desirable.

The motivation behind the current research is a desire to explore the possible application of CNT for biological sensors, which is a completely new dimension, which is under-explored. The ability to bind biomolecules selectively on the surface of the CNT, which result in a change in the transport properties of the CNT, is the goal behind this project. Also, the quantification of mass of the biomolecules bound on the surface by highly sensitive gravimetric sensors such as Quartz Crystal Microbalance. But in this process many other interesting facts were revealed. Raman spectroscopy of CNT showed temperature dependence with a significant change of signature. This was further explored by comparing the temperature dependence of SWNT and HOPG. A hypothesis is proposed to explain the anomalous behavior of SWNT owing to the structural difference of the two materials. This is a significant result in a state where efforts are being made to completely understand the properties and the behavior of these novel materials. An attempt to functionalize carbon nanotubes with different surfactants was made to improve the sensitivity of carbon nanotubes as biological sensors and to improve the solubility in aqueous solutions which are more feasible to be used in many applications. The treatment of CNT with certain surfactants made CNT highly protein resistant proving that the sensitivity of the CNT to biomolecules can be altered by surface

chemistry variations. As is the case with any other field, there is lot to be explored about these quantum wires be it the basic physics involved behind them or the applications of these in various fields. In conclusion, science has always been mysterious and exciting and so is it in the case of these novel materials. Man has always shown his supremacy in finding out the new secrets of nature be it THE COSMOS or THE CARBON NANOTUBE.

2.1. References

[1] H. W. Kroto, J. R. Heath, S. C. O' Brien, R. F. Curl, and R. E. Smalley, Nature, vol. 318, p. 162, (1985).

[2] P. J. F. Harris, "Carbon nanotubes and related structures", Cambridge University Press, Cambridge, (1999).

[3] T. Guo, P. Nikolave, A. G. Rinzler, D. Tomanek, D. T. Colbert, and R. E. Smalley, Chemical Physics Letters, vol. 243, p. 49. (1995).

[4] S. J. Tans, M. H. Devoret, H. Dai, A. Thess, R. E. Smalley, L. J. Geerligs, and C. Dekker, Nature, vol. 386, p. 474 (1997).

[5] N. Yao, and V. Lordie, Journal of Applied Physics, vol. 84, p. 1939, (1998).

[6] S. J. Tans, A. R. M. Verschueren, and C. Dekker, Nature, vol. 393, p. 49, (1998).

3. CARBON NANOTUBES: STRUCTURE, PREPARATION AND PROPERTIES

Carbon nanotubes can be broadly classified into two types

1. Single wall carbon nanotubes (SWNT)
2. Multi walled carbon nanotubes (MWNT)

SWNT can be imagined as a single graphene sheet rolled up into a seamless cylinder [1]. MWNT [2] structure is a bit more complex compared to SWNT. The simplest way to visualize a multi wall carbon nanotube is considering it as a coaxially arranged SWNT with increasing diameter just like a Russian doll.

In this research, we have used SWNT with an average diameter of ~1.4 nm. The structure and properties of single walled carbon nanotubes are discussed in much detail.

3.1. Structure of single walled carbon nanotubes

As discussed above SWNT are just graphene wrapped into a cylinder. Graphene is a polyaromatic mono-atomic layer made of hexagonal display of sp^2 hybridized carbon atoms. In sp^2 hybridization, there is a formation of three equivalent sp^2 hybrid orbitals, each holding one electron, would repel one another and take up the shape of a trigonal plane. The angles between the sp^2 hybrid orbitals are 120 degrees [3] as shown in Figure 3-1. All the three sp^2 hybrid orbitals lie on the single plane.

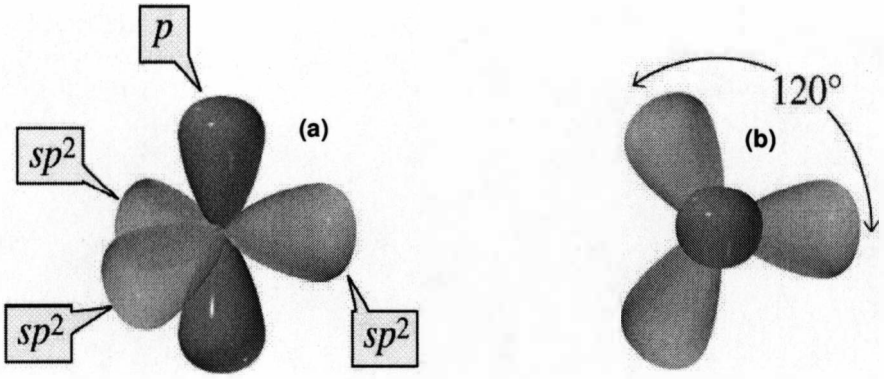

Figure 3-1. Schematic representation of SP^2 hybridization (a) Side view (b) Top view.

The remaining 2p (P_z) orbital is orientated perpendicular to this plane. However, the structure is not as simple as expected because of the infinite number ways this sheet can be wrapped to form a cylinder. The way a graphene sheet is rolled, indeed has a lot of importance because many properties of carbon nanotubes are very sensitive to this. Though geometry does not impose any restriction regarding the tube diameter, theoretical calculations suggest that the nanotubes crumple into two layer ribbons when the tube diameter is over 2.5nm. At the same time, extremely small diameters are possible but not often due to higher stress and the higher energy cost for tubes of extremely small diameter (0.3nm) [4]. Taking the above two factors into consideration, the best compromise for the tube diameter is found to be at ~1.4 nm. There are no restrictions on the length of the nanotubes and recently nanotubes of 1.4nm diameter with a length of 100 meters have been synthesized.

Figure 3-2 represents a single sheet of graphene. The numerous ways to roll this sheet of graphene is defined mathematically by the chirality vector C_h The chirality vector is shown below.

$$OA = C_h = na_1 + ma_2$$

$$a_1 = \frac{a\sqrt{3}}{2}x + \frac{a}{2}y$$

$$a_2 = \frac{a\sqrt{3}}{2}x - \frac{a}{2}y$$

$a=0.246nm$

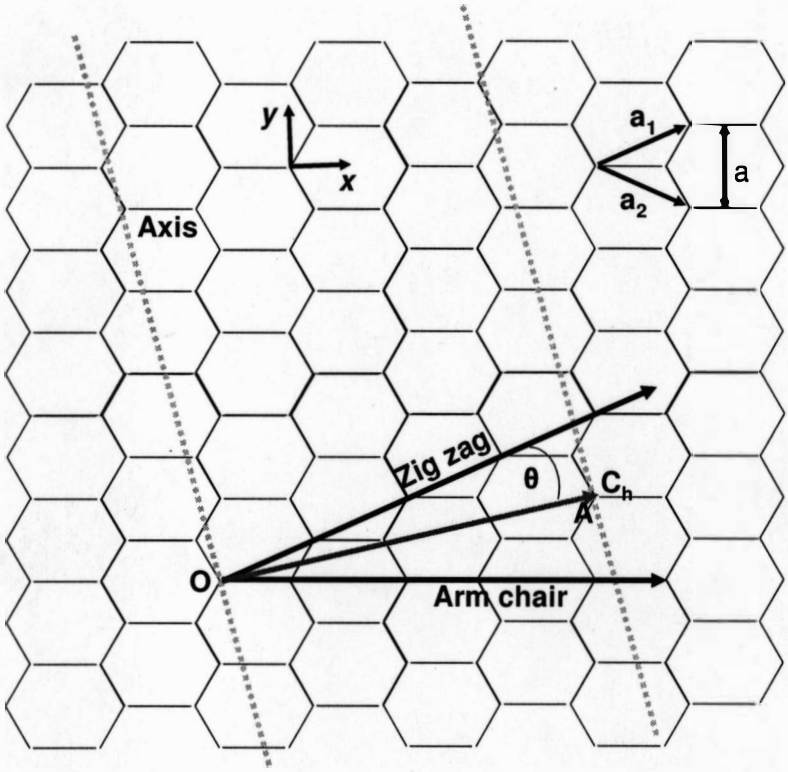

Figure 3-2. Schematic of a structure of SWNT from a graphene sheet.

From basic geometry the chiral angle (Θ) can be derived.

$$\cos\theta = \frac{2n+m}{2\sqrt{(n^2+m^2+nm)}}$$

The relation of the diameter of the nanotube in terms of n, m is as follows

$$D = \frac{|C_h|}{\pi} = \frac{a_{CC}\sqrt{3(n^2+m^2+nm)}}{\pi}$$

Since all the parameters governing the structure of a SWNT can be uniquely determined by knowing the n and m values. Thus SWNTs are also designated as (n, m) nanotube. Figure 3-3 shows the structure of different carbon nanotubes with different (n, m) values. In the Figure (2, 2) and (10, 10) are called armchair nanotubes for which n=m. (5, 0) tube is a zig-zag tube where m=0 and the last one is the example of chiral tube where n≠m and m≠0.

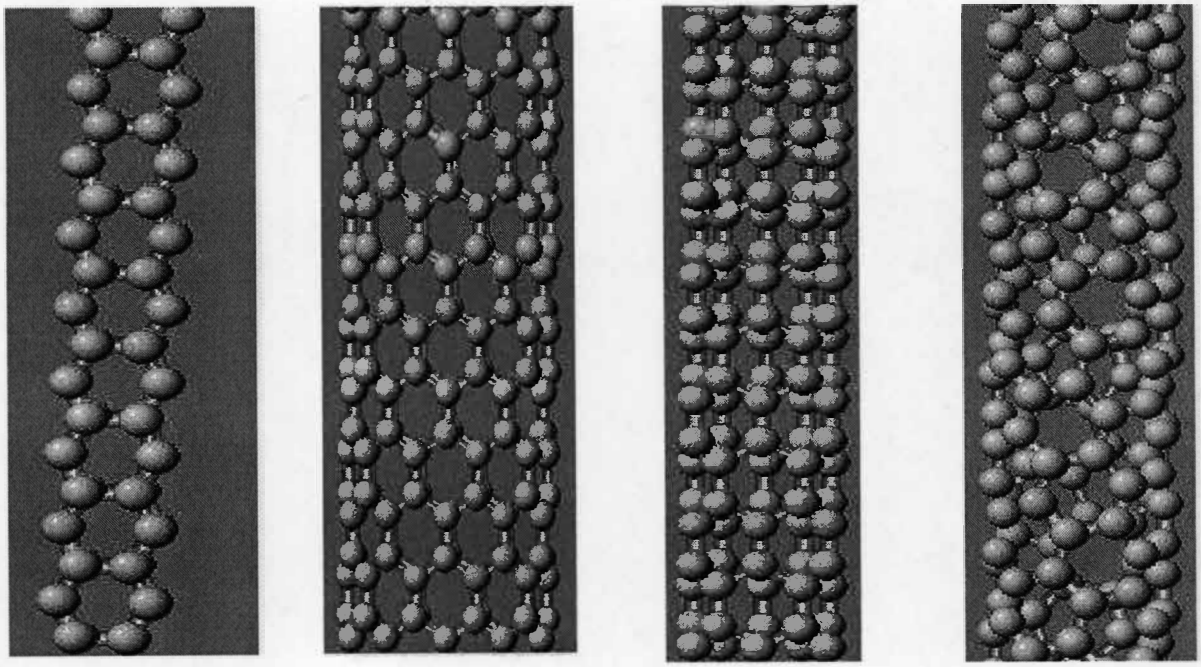

Figure 3-3. Structure of different types of carbon nanotubes (a) (2, 2), (b) (10, 10), (c) (5, 0), and (d) (5, 2).

3.2. Preparation of carbon nanotubes

Carbon nanotubes can be synthesized by several techniques like electric arc discharge, laser ablation, catalytic chemical vapor deposition and template based manufacturing. Although there are few other miscellaneous techniques these are considered as the most important and reliable ways of synthesizing carbon nanotubes, which are briefly described.

3.2.1. Electric arc discharge method

In this technique [5], carbon is vaporized in the presence of catalyst like iron, nickel, yttrium etc. the vaporization is carried out in a special chamber with reduced atmosphere (~600mbar) of noble gas like argon or helium. An electric arc is triggered between two electrodes, which cause the formation plasma consisting of carbon vapor, inert gas and the vapor of catalyst as shown in Figure 3-4. The vaporization is due to the energy transfer from arc to the anode made of graphite doped with catalyst particles. Then the carbon nanotubes are deposited in different parts of the furnace like the walls of the chamber, cathode and so on.

The discovery of CNT [6] by Iijima was by this technique. He collected the soot material from the cathode and studied it with Transmission Electron Microscopy (TEM). Although he found MWNT in these studies, the same technique was later extended to SWNT synthesis. The disadvantage of this method is that there is a high proportion of catalyst residue, which forms the impurity. The nanotubes produced by this method have a wide distribution of diameter and properties.

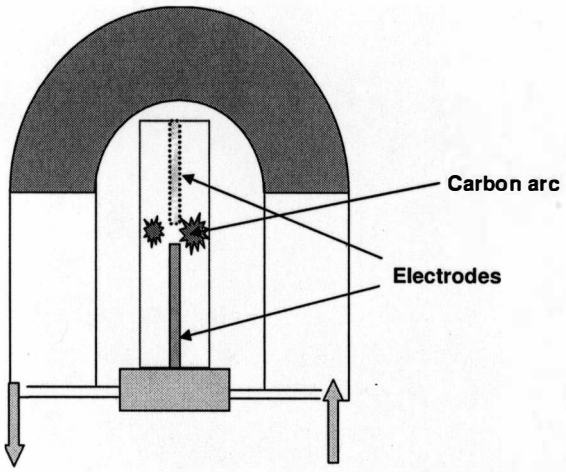

Figure 3-4. Schematic of arc discharge method for synthesis of CNT.

3.2.2. Laser ablation method

The laser ablation method was initially used for production of C_{60} molecule [7], which is considered as the parent molecule in the fullerene family. Figure 3-5 elucidates the principle involved in the preparation of carbon nanotubes by laser ablation. A graphite target doped with a catalyst is placed in the middle of a noble gas filled quartz tube. The laser beam is focused on to the graphite source and this focused laser vaporizes and sublimes the graphite by uniformly bombarding the surface [8].

The nanotubes are collected on the cold collector placed in the quartz tube. When a carbon source without catalyst material is used in laser ablation multi walled carbon nanotubes are formed. Electric arc discharge and laser ablation methods have two things in common. Firstly, a high temperature requirement and secondly, the carbon originates form the erosion of solid graphite.

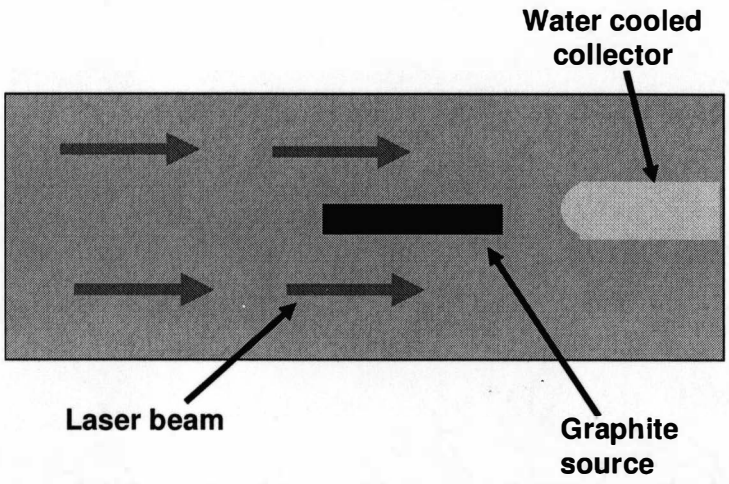

Figure 3-5. Schematic of laser ablation method for synthesis of CNT.

3.2.3. Catalytic chemical vapor deposition

This method is based on the decomposition of the gaseous form of carbon (hydro carbons like methane) on catalyst particles inside the chemical vapor deposition chamber [9]. The catalyst particles usually used are iron, cobalt and nickel. The advantage of this process is that it is a low temperature process compared to the other two methods. Carbon nanotubes produced by this method are much longer compared to the arc discharge methods. Recently, carbon nanotubes of 100m long were produced by this method. The aspect ratio of these tubes is nearly 10^{12}. To conclude with, the growth process of carbon nanotubes is yet not fully understood. This is the one of the main problems nanoscience is facing today. All the known methods of fabricating carbon nanotubes give a wide variety of tubes with different properties [10]. It is a tedious task to separate them and use them for specific applications like interconnects and active devices and so on.

3.3. Properties of carbon nanotubes

Carbon nanotubes possess unique electrical, mechanical and thermal properties, which make carbon nanotube the most promising and nanostuctured materials. Few properties, which place carbon nanotubes in the foremost place in the field of nanotechnology, are discussed here.

3.3.1. Electrical properties

Nanoscale structures often have dimensions smaller than electron scattering lengths [11]. Carbon nanotubes are the best examples for such kind of materials. This makes carbon nanotubes exhibit ballistic transport properties. It means that if an electron enters the nanotube, it can then travel without any resistance through the nanotube molecule. The nanotube is so defect-free that it doesn't scatter back, which is where normal resistance comes from. So, they can act as wave-guides for electrons. Depending on their chirality carbon nanotube behave as metals and moderate band gap semiconductors. In fact carbon nanotubes are the only molecules known to science that exhibit metallic behavior at single molecule level. Carbon nanotubes can transport very high current densities like $10^9 A/cm^2$ [10]. This current density is very high compared to even best conductors like copper. Carbon nanotubes exhibit metallic properties when

$$n\text{-}m = 3q \text{ where q is an integer.}$$

For all other values of n, m the nanotubes behave as semiconductors [10]. All armchair nanotubes (i.e. tubes for which n=m) behave as metals. It is well known that the conduction band and the valance band of the single graphene sheet superimpose at six corners of Brillouin zone. When this sheet of graphene is rolled to form a tube, the

periodic boundary conditions overlap to form one-dimensional sub-bands. This particular phenomenon makes carbon nanotubes ideal systems for the study of quantum confinement effects and 1-D charge transport [12]. One more interesting aspect that is worth mentioning is that any mechanical stress or deformation of carbon nanotubes causes alteration in their subbands that directly influence their transport properties. So it is possible to finely tune the electronic properties of carbon nanotube by mechanical deformation [13]. As discussed earlier, there is no technique in practice till date to fabricate carbon nanotubes with desired electronic properties.

3.3.2. Mechanical properties

Although tubular morphology at nanoscale is observed for many 2-D solids, nanotubes are unique because of the sp^2 hybridization, which is particularly a strong three folded bonding. This special property of carbon nanotubes makes them stronger than diamond, which is believed to be one of the strongest materials. The tensile strength of carbon nanotubes is very high and it is almost 20 times higher than steel and it has been measured to be 45Gpa [14]. Tensile young's modulus of MWNT is highest recorded so far for any material, the value being 1Tpa [15].

3.3.3. Thermal properties

The thermal properties of carbon nanotubes are directly related to their unique structure and small size. Because of these properties, nanotubes are proved to be an ideal material for the study of low-dimensional phonon physics, and for thermal management, at nanoscale. The thermal properties of carbon nanotubes are not completely understood as yet. There is some disagreement into the exact nature of the thermal conductivity of

carbon nanotubes, although most of them agree that thermal conductivity seems to change depending on temperature, and possible also on current and vacancy concentration. It was suggested that the conductivity was linear in temperature from 7 K to 25 K [16]. From 25 K to 40 K, the line increases in slope, and it arises monotonically with temperature to above room temperature. The thermal conductivity of CNT competes with diamond or a single sheet of graphite, which are regarded as the best heat conductors. The thermal conductivity of even aligned bundles of SWNTs (the form of nanotubes used in this research) is > 200W/m K [16] at room temperature.

With such highly desirable properties CNTs can find applications in many different fields. This electronic properties of nanotubes makes them the ideal choice for interconnects and also as active devices of nanoelectronics. CNTs can be used as fillers in polymer and ceramic nanocomposites for improving the mechanical strength and electrical conductivity of composites. CNT based field emission devices [17] are commercially available and have proven to be much more efficient compared to the traditional field emitters. Carbon nanotubes can also be used as tips [18] for scanning probe microscopes. Due to their extremely small radius of curvature they can produce high-resolution images compared to the tips produced by silicon micro machining.

In summary this chapter introduces the structure of carbon nanotubes, which are basically graphene sheets, wrapped into cylinders. This chapter dealt with the few important preparation methods of CNT like the arc discharge, laser ablation and chemical vapor deposition. Also the most important properties like the miniature size and the electrical conductivity and applications of carbon nanotubes have been the motivation behind this work, were discussed.

3.4. References

[1] J. Tersoff, and R. S. Ruoff, Physics Review Letters, vol. 73, p. 676 (1994).

[2] H. Allouche, and M. Monthioux, Carbon, In Press, (2003).

[3] R. T. Morrison, and R. N. Boyd, "Organic Chemistry", Allyn and Bacon, Boston, (1973).

[4] X. Zhavo, Y. Liu, S. Inoue, T. Suzuki, R. O. Jones, and Y. Ando, Physics Review Letters, vol. 92, p. 125502-1, (2004).

[5] W. Kratschmer, L. D. Lamb, K. Fostirotoulos, and D. R. Hauffman, Nature, vol. 347, p. 354, (1990).

[6] S. Iijama, Nature, vol. 354, p.56, (1991).

[7] H. W. Kroto, J. R. Heath, S. C. O' Brien, R. F. Curl, and R. E. Smalley, Nature, vol. 318, p. 162, (1985).

[8] T. Guo, P. Nikolave, A. Thess, D. T. Colbert, and R. E. Smalley, Chemical Physics Letters, vol. 243, p. 49, (1995).

[9] G. G. Tibbets, M. Endo, and C. P. Beetz, Sampe J, vol. 27, p. 315, (1989).

[10] J. W. G. Wildoer, L. C. Venema, A. G. Rinzler, R. E. Smalley, and C. Dekker, Nature, vol. 391, p. 59, (1998).

[11] P. L. Mc Euen, M. S. Fuhrer, and H. Park, IEEE Transactions on Nanotechnology, vol. 1, p. 78, (2002).

[12] S. J. Tans, M. H. Devoret, H. Dai, A. Thess, R. E. Smalley, L. J. Geerligs, and C. Dekker, Nature, vol. 386, p. 474, (1997).

[13] E. D. Minot, "Tuning the band structure of carbon nanotubes", Ph. D. Thesis, Cornell University, Aug, (2004).

[14] D. A. Walters, L. M. Ericson, M. J. Casavant, J. Liu, D. T. Colbert, K. A. Smith, and R. E. Smalley, Applied Physics Letters, vol. 74, p. 3803, (1999).

[15] N. Yao, and V. Lordie, Journal of Applied Physics, vol. 84, p. 1939, (1998).

[16] J. Hone, and M. Whitney, A. Zettle, Synthetic Metals, vol. 103, p. 2498, (1999).

[17] W. A. DeHeer, A. Chatelain, and B. Ugarte, Science, vol. 270, p. 1179, (1995).

[18] S. S. Wong, E. Goselevich, A. T. Woodley, C. L. Cheung, and C. M. Lieber, Nature, vol. 394, p. 52, (1998).

4. CHARACTERIZATION TOOLS

4.1. Atomic force microscopy

Atomic force microscopy (AFM) [1] falls into the family of Scanning Probe Microscopy (SPM). Scanning Tunneling Microscopy (STM) [2] is the first type of SPM invented in early 1980's by Gerd Binnig and Heinrich Rohrer of IBM Zurich Laboratories. Gerd Binnig received a Nobel Prize in physics in 1986 for this invention. In Scanning Tunneling Microscopy, a very sharp conductive needle scans across the sample with atomic separation between the sample and the needle. A bias voltage is applied to the needle and the sample is grounded or vice versa. The tunneling current between the needle and the sample because of the quantum tunneling effect acts as a measure for the height distribution of the sample. A feedback loop controls the needle distance from the sample surface based on the tunneling current. The STM has a vertical resolution of 1Å which is close to the dimension of an atom.

However, the disadvantage of a STM is that the sample needs to be conductive which is not always true. To overcome this difficulty, the same technique is slightly modified and implemented with the help of force feedback. Binning and Quarte invented the technique in 1986 again from IBM laboratories [1]. This kind of microscopy is called Atomic Force Microscopy. In this work, a Thermomicroscopes (Autoprobe CP Research machine) has been used. In Atomic Force Microscopy, a mechanically flexible cantilever with a sharp tip scans across the sample with some fixed force. The cantilever moves in Z direction in order to maintain the same force of interaction [3]. Usually, the forces are atomic forces

of interaction (e.g. van der Waal forces). Figure 4-1 shows the picture of the cantilever with the tip scanning across the sample.

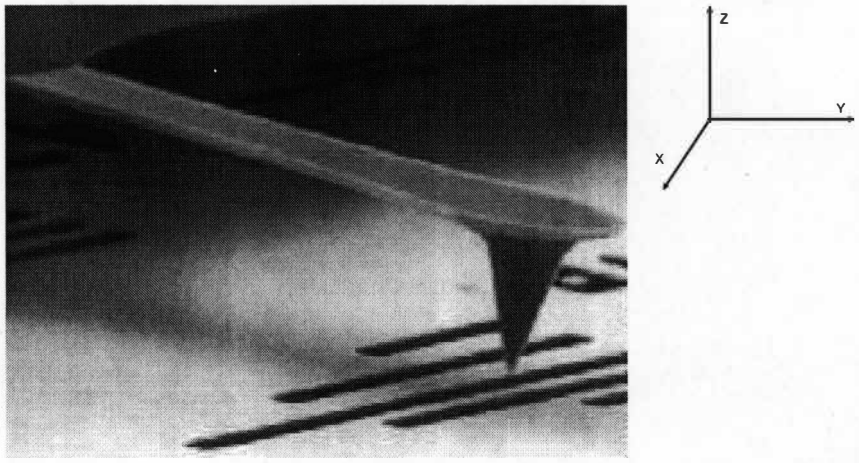

Figure 4-1. SEM image of the cantilever with the tip and the axis direction.

The length of the cantilever is approximately 100μm and the length of the tip is 5-10μm. The radius of curvature of the tip is about 10nm. In fact, radius of curvature of the tip is the only limiting factor of the resolution of AFM. The cantilever with the tip, which is the probe in the case of AFM, is fabricated by micro machining technologies. Commonly used tip materials are silicon or silicon nitride. However, for special applications like Magnetic Force Microscopy the tips are coated with magnetic materials like cobalt.

There are three very common modes of AFM.

1. Contact mode
2. Non contact mode
3. Tapping mode

4.1.1. Contact mode

In contact mode of AFM, the tip actually is in contact with the sample. A constant force is maintained by the tip on the sample and this force is chosen depending on many factors like type of the sample, material with which the tip is made, spring constant of the cantilever beam and so on. A laser beam is focused onto the back of the cantilever. This laser reflected from the cantilever surface that is captured by a split photodiode and the electrical signal generated by the photodiode is in direct correspondence to the cantilever bending. Contact mode of AFM provides the best resolution, however, sample is prone to damage in contact mode microscopy. Besides imaging, contact mode of AFM can also be used for nanomanipulation, nanolithography and so on. Nanolithography is the art of writing patterns on the sample with the AFM tip. The Figure 4-2 above shows the letters "WMU" written with the AFM tip by erasing thermally evaporated silver on silicon surface.

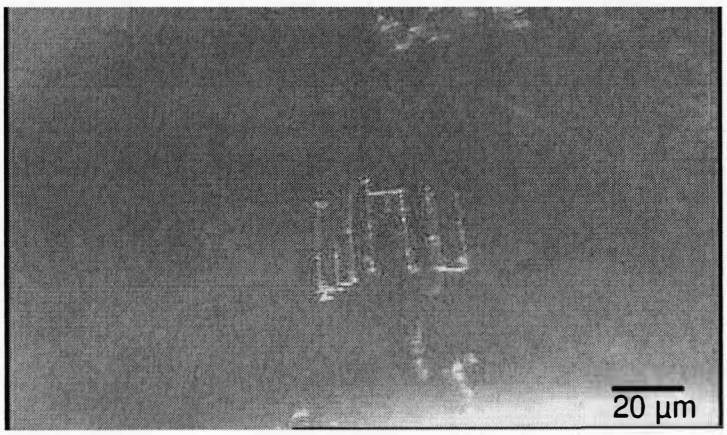

Figure 4-2. Optical micrograph showing the letters "WMU" written with AFM tip.

4.1.2. Non-contact mode

Non-contact mode of AFM is one of the most widely used methods. As discussed earlier, contact mode is not a very good choice for studying soft and elastic samples because of the chances of getting damaged. To overcome this drawback, non-contact mode of microscopy was invented in which the tip is at a finite distance from the sample during scanning. Normally the tip is separated form the sample by a distance of 50 to 150 Angstroms [4]. In this case the attractive van der Waals forces acting between the tip and the sample are detected and topography is constructed by scanning the tip above the surface. But the van der Waal forces are much weaker compared to the mechanical forces in the case of contact mode. This is compensated by oscillating the cantilever slightly above its resonant frequency with amplitude of appriximately10nm. Nevertheless tip does not touch the sample but the damping of the oscillations due to the interaction between the first atom of the sample and the last atom the tip are detected and encoded as a 3D topography image of the sample. In short, long-range van der Waal forces reduce the amplitude of oscillation by effectively shifting the spring constant experienced by the tip and changing its resonant frequency. Unless specified, most of the AFM imaging performed in this work was performed in non-contact mode.

4.1.3. Tapping mode

Tapping mode is similar to non-contact mode except that in this the tip touches sample intermittently once in every cycle. So in this case, ionic repulsive forces as in contact mode reduce the amplitude [5]. Tapping mode is also called as intermittent mode of AFM.

4.2. Raman spectroscopy

Raman and Krishnan, two Indian physicists discovered the Raman Effect in 1928 [6]. This technique can be used to identify and quantify samples based on the molecular vibrations information obtained. Raman spectrometers can be generally classified into three categories: single channel photomultiplier tube based systems, multichannel spectrometers based on intensified photo diode array and charged couples devices based multichannel systems [7].

4.2.1. Principle

Raman spectroscopy is based on the phenomenon of light scattering in which the incidental photons are destroyed and their energy is used for creating scattered photons. The part of energy lost by the photons is used in the creation (Stokes process) or destruction (anti-Stokes process) of vibrations in the studied sample. When a sample (of course it is a group of molecules or atoms) is subjected to light most photons are elastically scattered, a process called Rayleigh scattering. A small portion of the photons are scattered in elastically i.e. the energy of the incident photon is different from that of the scattered photon [8]. The mechanism of Raman spectroscopy is based on the phenomenon of light scattering, in which electromagnetic radiation interacts with an oscillating, polarizable electron cloud of an atom or molecular group [8]. Light is scattered due to non-resonant interaction between photons and electrons of an atom. Most of the incident radiation refracted, transmitted or scattered remains unchanged in frequency (energy) when an incident photon interacts with a molecule or group of molecules. The fraction of the energy lost to the vibrational energy levels appears as Raman scattered radiation. When an exiting photon transfers a fraction of its energy to a

vibrational level of the system Stokes Raman scattering occurs and when it gains energy anti-Stokes Raman scattering occurs. The frequencies which fall into stokes and anti-stokes are shown in Figure 4-3. When the frequency of the scattered light is same as that of the incident photon, Rayleigh scattering occurs.

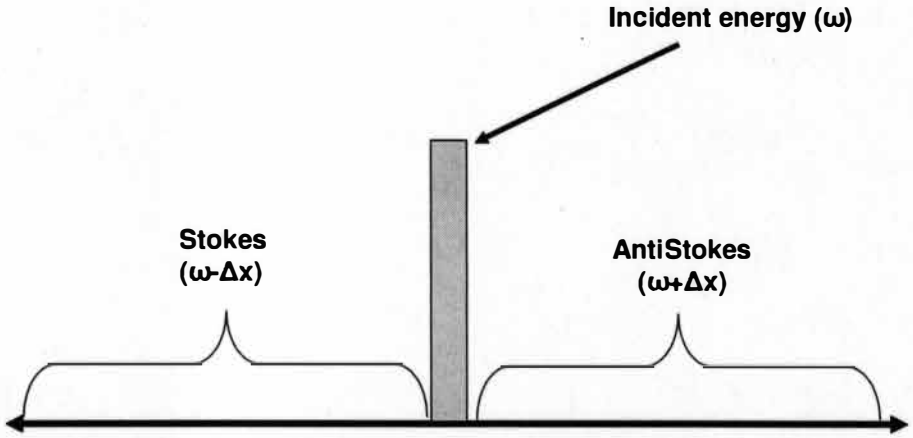

Figure 4-3. Raman scattering frequencies for stokes and anti-stokes.

4.2.2. Instrumentation

Figure 4-4 shows the block diagram of a Raman spectrometer. The sample to be examined is irradiated with intense monochromatic light (laser) after passing through a line filter to remove any unwanted laser lines and sidebands. The wavelength of laser should be as small as possible since the Raman scattering cross section varies as the fourth power of the frequency. The laser passes through a beam splitter and a microscope lens that focuses the laser light onto a small diffraction limited spot on the sample. The scattered light from the sample is transmitted through a fiber optic interface between the sample and optical processing system (spectrometer). Based on the frequency components, the optical processing system characterizes the collected light.

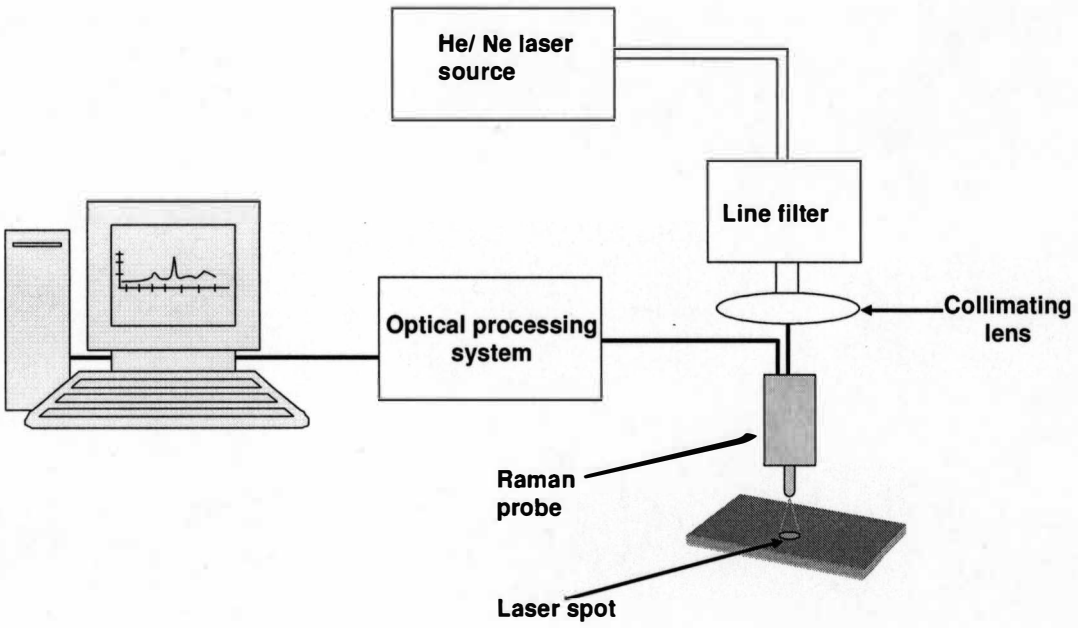

Figure 4-4. Block diagram of the Raman spectrometer setup.

4.2.3. Surface Enhanced Raman Spectroscopy (SERS)

The discovery of SERS is a major breakthrough in Raman detection capabilities. Surface Enhanced Raman Spectroscopy (SERS) is a Raman Spectroscopic (RS) technique that provides greatly enhanced Raman signal from Raman-active analyte that has been adsorbed onto certain specially prepared metal surfaces. The transitions due to vibrations in molecules adsorbed on rough metallic substrate excited by a laser source enhance the Raman cross section by a factor of 10^6. The reason behind this is the resonance-related effects and large optical fields. The importance of SERS is that the surface selectivity and sensitivity extends Raman Spectroscopy characterization to a wide variety of interfacial systems previously inaccessible to RS because RS was not surface sensitive.

There are two primary mechanisms for the enhancement in intensity: electromagnetic and chemical enhancement. The electromagnetic effect is dominant of the two. The chemical

effect contributes enhancement only on the order of one or two magnitude. The electromagnetic enhancement (EME) is dependent on the presence of the metal surface's roughness features, while the chemical enhancement (CE) involves changes to the adsorbate electronic states due to chemisorption of the analyte.

The intensity of Raman signal is proportional to the square of the electromagnetic field on the analyte molecule.

$$I \propto E_a^{\,2} \qquad (1)$$

The Electromagnetic field of the excitation radiation is incident on the analyte. This is the case for normal Raman scattering and the E_a is relatively small since the source of the Electromagnetic radiation is relatively far away (the laser).

So for normal Raman scattering

$$I \propto E_a^{\,2} \qquad (2)$$

In SERS, the presence of the roughness feature provides another Electromagnetic field that is of the metal particle itself, E_p, and this Electromagnetic field is quite proximate as the analyte is adsorbed onto the roughness feature, of which the surface is composed. Because of this proximity, any Electromagnetic field from the metal particle will contribute a large factor to E (= E_a+E_p). Now the intensity is proportional to the square of the sum of E_a and E_p

$$I \propto (E_a + E_p)^2 \qquad (3)$$

Thus the signal of the Raman Spectroscopy can be greatly enhanced by adsorbing the analyte molecule on the atomic scale rough metal surface.

4.3. Quartz Crystal Microbalance

4.3.1. Principle

Quartz Crystal Microbalance (QCM) falls into the category of Bulk Acoustic Wave (BAW) resonator. Bulk acoustic wave resonators consist of piezoelectric quartz crystals with metal electrodes on either side. Application of a radio frequency signal to the electrodes causes excitation of a shear mechanical resonance. The crystals resonate at its resonant frequency (in this study 5 MHz crystals were used). Materials in contact with the quartz surface interact mechanically and perturb the resonant frequency. If a mass is adsorbed on the electrodes, and if the adsorbed mass is small compared to the mass of the crystal, evenly distributed and rigidly attached, with no slip or deformation due to the oscillatory motion of the crystal, the resonant frequency of the crystal decreases proportionally to the mass bound on the surface [9].

The change in the resonant frequency and the mass bound on the surface are related by a simple proportionality equation which is popularly known as the Sauerbrey equation [10]

$$\Delta f = \frac{-2 f_0^{\,2} \Delta m}{A\sqrt{\rho_q \mu_q}}$$

where f_0 is the fundamental resonant frequency, A is the piezoelectrically active area defined by the two gold electrodes, ρ_q is the density of quartz (2.648 g cm^{-3}) and μ_q is the shear modulus (2.947 x 10^{11} dyn cm^{-2}). Sauerbrey equation is based on an assumption

that the mass has been rigidly attached to the crystal and has negligible thickness as compared to the crystal as a whole.

In summary, this chapter briefly introduced the various tools used through out the research. It is very important to understand the physical phenomenon behind various analytical tools in the nanoscience research. The operating principle of AFM, Raman spectroscopy, surface enhanced Raman spectroscopy and QCM, basically a gravimetric sensor, which is a strong quantization tool, was also introduced.

4.4. References

[1] G. Binning, C. F. Quarte and C. H. Gerber, Physical Review Letters, vol. 56, p. 930, (1985).

[2] G. Binning, and H. Rohrer, Helvetica Physica Acta, vol. 55, p. 726, (1982).

[3] S. H. Cohen, and M. L. Lightbody, "Atomic force microscopy/scanning tunneling microscopy", Plenum Press, New York, (1997).

[4] F. J. Giessibl, Review of modern physics, vol. 75, p. 949, (2003).

[5] S. Morita, R. Wiesendanger, and E. Meyer, "Non-contact atomic force microscopy", Springer, Berlin, (2002).

[6] C. V. Raman, and K. S. Krishnan, Nature, vol. 121, p.501, (1928).

[7] J. J. Laserna, "Modern Techniques in Raman Spectroscopy", John Wiley & Sons, (1996).

[8] A. H. Kuptsov, G. N. Zhizhin, "Handbook of Fourier Transform Raman and Infrared Spectra of Polymers", Elsevier, (1998).

[9] P. Ihalainen and J. Peltonen, Sensors and Actuators B, vol. 102, p. 207, (2004).

[10] G. Sauerbrey, Z. Phys, vol. 55, p. 206, (1959).

5. PURIFICATION AND CHARACTERIZATION OF CARBON NANOTUBES

5.1. Introduction

Carbon nanotubes can be fabricated in a number of different ways like arc discharge [1], laser ablation [2] and chemical vapor deposition [3] by breaking down hydrocarbon gases. In most of the cases, the growth of the carbon nanotubes is facilitated only in the presence of a catalyst like nickel and yttrium. So the carbon nanotubes synthesized in these methods invariably have the catalyst particles and amorphous carbon as impurities. Carbon nanotubes used in the research were purchased from carbolex Inc. The as purchased carbon nanotubes were 70% pure with yttrium and nickel being the residue.

5.2. Purification of the carbon nanotubes

The carbon nanotubes were dissolved in organic solvents like chloroform and then the solution was casted on the silicon substrates. AFM imaging was performed to understand the impurity level and the distribution of the nanotubes on the surface of the substrate. Figure 5-1 shows the AFM image of the carbon nanotubes casted on silicon substrate. It can be seen from the AFM image that most of the surface is covered with particles of nickel and amorphous carbon. The size of the nickel particles was approximately 50nm. It was difficult to locate carbon nanotubes in the casted samples.

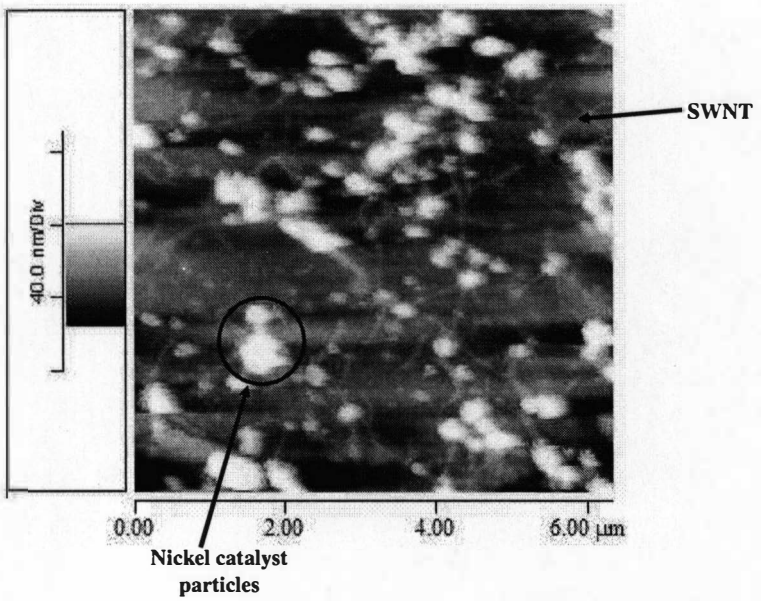

Figure 5-1. AFM micrograph of as purchased CNT casted silicon substrate.

In order to confirm the presence of carbon nanotubes, two methods were chosen. Raman spectroscopy was one of the methods opted. Figure 5-2 shows the Raman spectrum of the casted CNT sample.

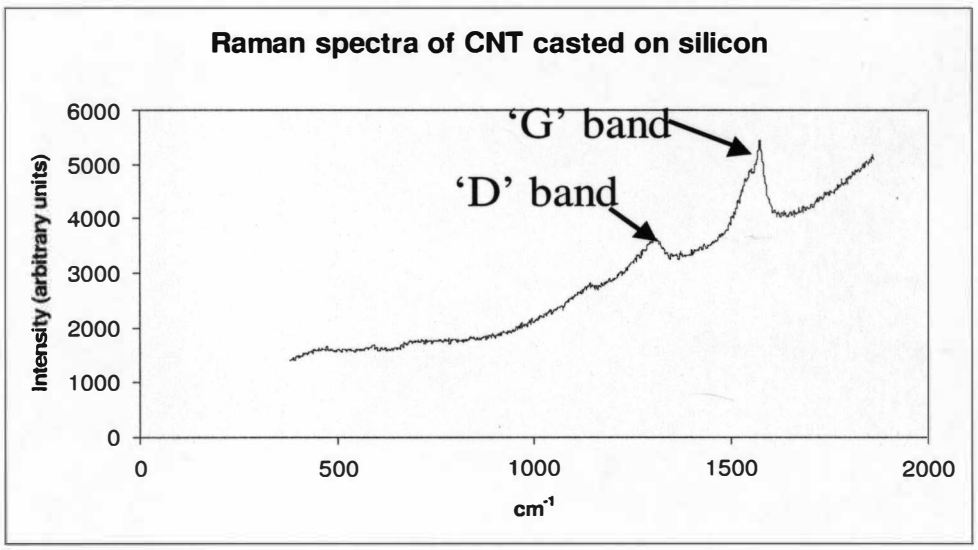

Figure 5-2. Raman spectrum of casted carbon nanotubes on glass substrate.

The spectrum showed the characteristic 'G' band and 'D' band peaks of the carbon nanotube at approximately 1590 cm^{-1} and 1350 cm^{-1} respectively[4].

Also, AFM imaging was performed on silicon substrates with the CNT dip coated from the CNT solution. Figure 5-3 shows the AFM image of the sample dip coated from the solution. From the image, it can clearly be seen that a lot of carbon nanotubes have been deposited on the substrate. It can also be observed that there are a lot of catalyst particles in the purchased carbon nanotubes.

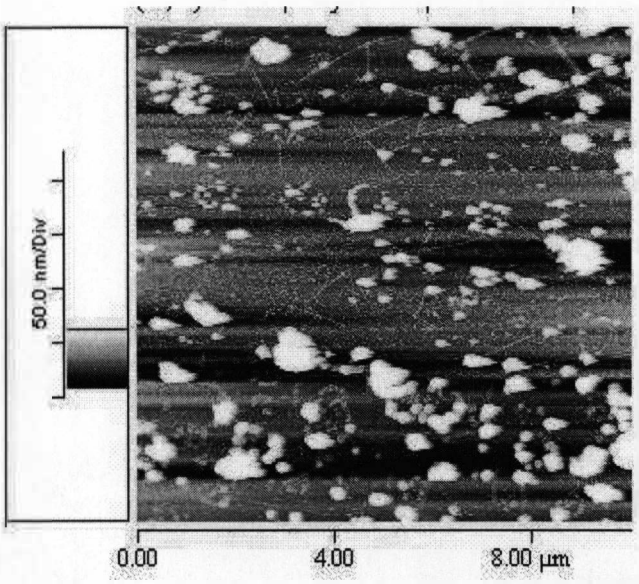

Figure 5-3. AFM micrograph of silicon substrate dip coated with CNT solution.

As a first step towards the possible application of CNT for chemical and biological sensing, it is important to eliminate these impurities. The purification was performed in two different ways. In the first method, the nanotube solution was centrifuged at 14000rpm for 30 min.

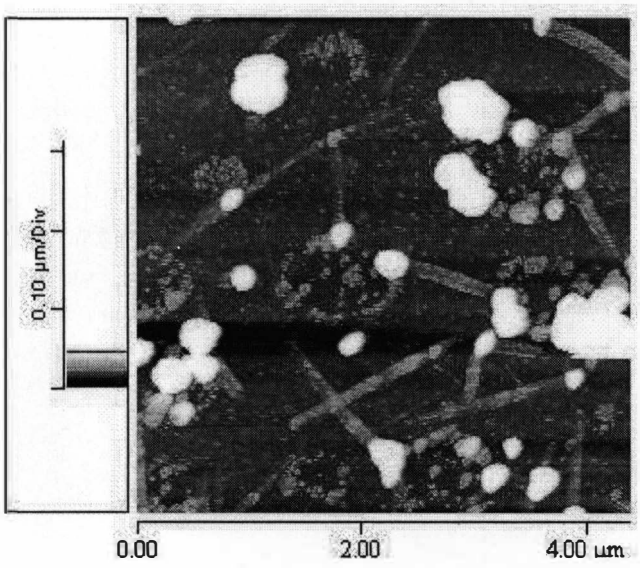

Figure 5-4. AFM image of CNT purified by centrifusion technique.

During the centrifuging process, the nickel particles which were comparatively denser than the carbon nanotube, settled at the bottom. The top three quarters of the solution was carefully separated and casted on the silicon substrates. Figure 5-4 shows the AFM image of the sample which showed a considerable improvement in the level of purity but still had some quantity of the impurity. The purity level achieved in this method is not enough to use the carbon nanotubes for critical experiments like biomolecule immobilization and as chemical sensors because the catalyst partcles might significantly influence the performance of the sensors.

The second method of purification involves using an anatop molecular filter to filter out the unwanted catalyst particles. The filters were purchased from Whatman Co. and the pore diameter was 20nm. CNT were dissolved in organic solvents like chloroform and then the solution was filtered through the anatop filters. Figure 5-5 shows the carbon nanotube/chloroform solution before and after filtration. It can be seen that the solution had a black tint before filtration and lost the tint during the process of filtration.

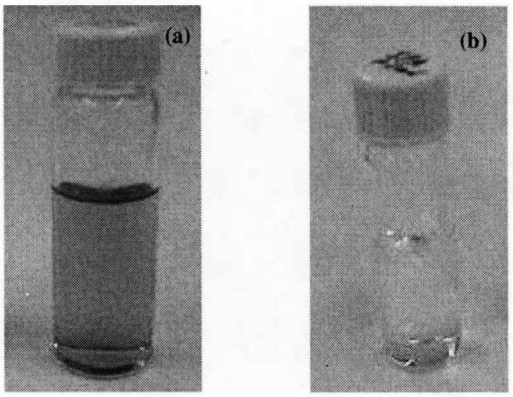

Figure 5-5. Carbon nanotube samples pictures (a) before and (b) after filtration.

The filtered carbon nanotube solution was then casted on silicon substrates and AFM imaging was performed to check the purity levels of the solution. It can be observed from the AFM image of Figure 5-6 that except for the amorphous carbon contamination most of the impurities were filtered. It can also be seen that the carbon nanotube bundles into a rope which is their natural tendency. This is because of the Vander wall forces of attraction between the tubes [5].

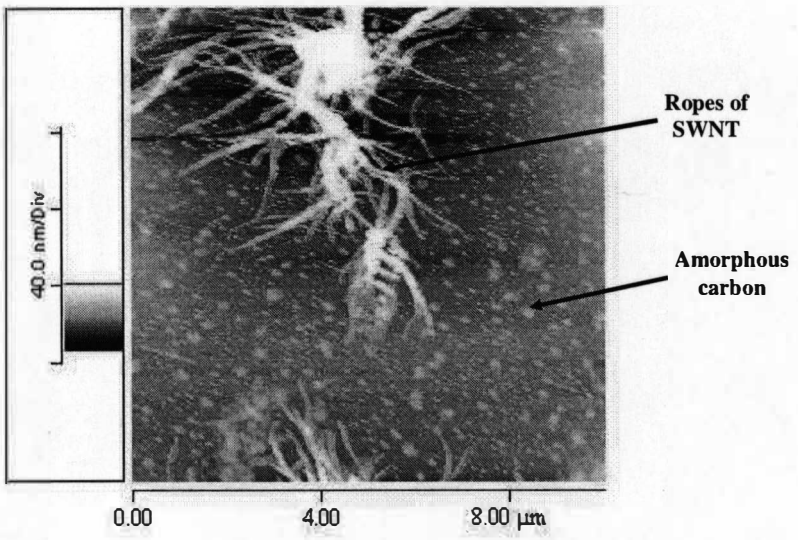

Figure 5-6. AFM micrograph of the carbon nanotubes casted from the filtered solution on silicon substrate.

The solution was then placed in an ultrasonic bath and agitated for 20 min to separate the ropes of nanotube in to individual tubes. The ultrasonically agitated solution was then casted on silicon substrates and the imaging revealed that the tubes were separated into individual tubes spread out on the substrates resulting in highly pure and uniform matrices of SWNT as shown in Figure 5-7.

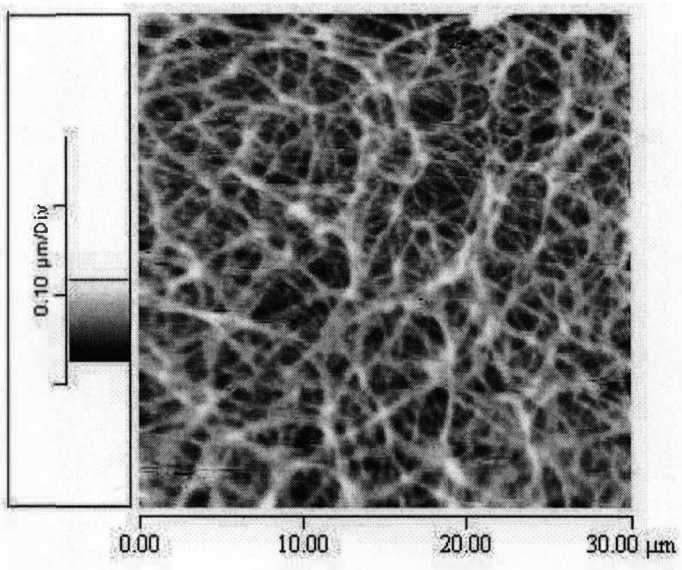

Figure 5-7. AFM micrograph of the carbon nanotube casted the filtered solution after ultrasonic agitation.

5.3. Characterization of carbon nanotubes

5.3.1. AFM imaging of carbon nanotubes

AFM imaging of carbon nanotubes was performed by casting them from solutions of various organic solvents. In order to measure the average diameter of the carbon nanotubes the solutions were highly diluted and sonicated for two hours before casting. AFM images revealed an average diameter of carbon nanotube to be 1.4 nm. This was confirmed after a number of samples. Figure 5-8 shows two carbon nanotubes

intertwined to form a bundle. However, it can be seen that the bundle is deroped at the end and individual nanotubes can be seen. Height profile of the tubes shows that both the nanotubes are 1.4 nm in diameter.

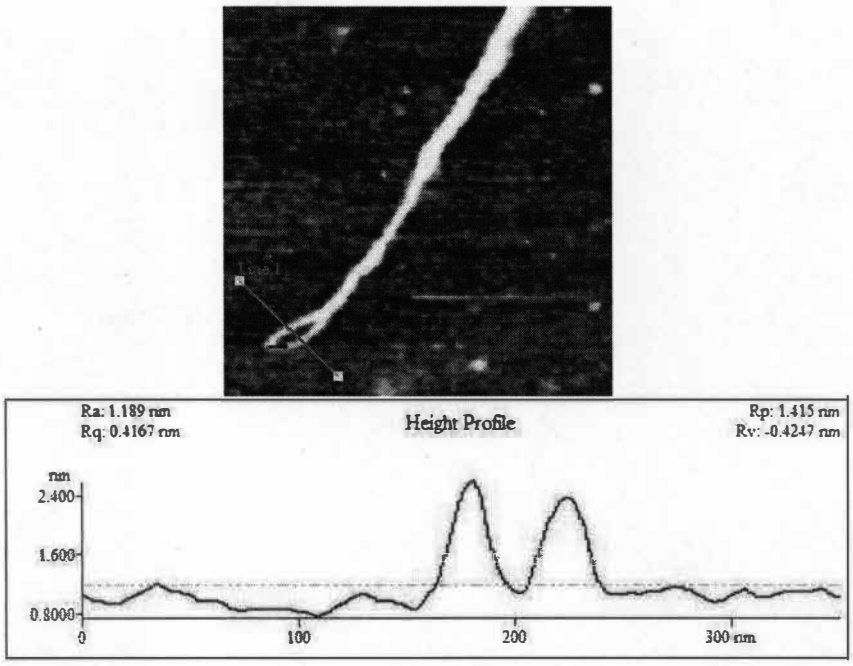

Figure 5-8. AFM image and height profile of CNT on silicon substrate.

The biological and chemical sensors in this work are fabricated by ultra thin films of carbon nanotubes. Films of desired thickness were formed by varying the concentration and the amount of the solution casted on the substrate. The thickness of these films was measured by AFM. For measuring the thickness of the film, a scratch was made on the CNT film with the AFM tip by scanning in contact mode. Then AFM imaging was performed across this scratch to measure the thickness. Figure 5-9 shows the AFM image of the CNT film with a thickness of 20nm.

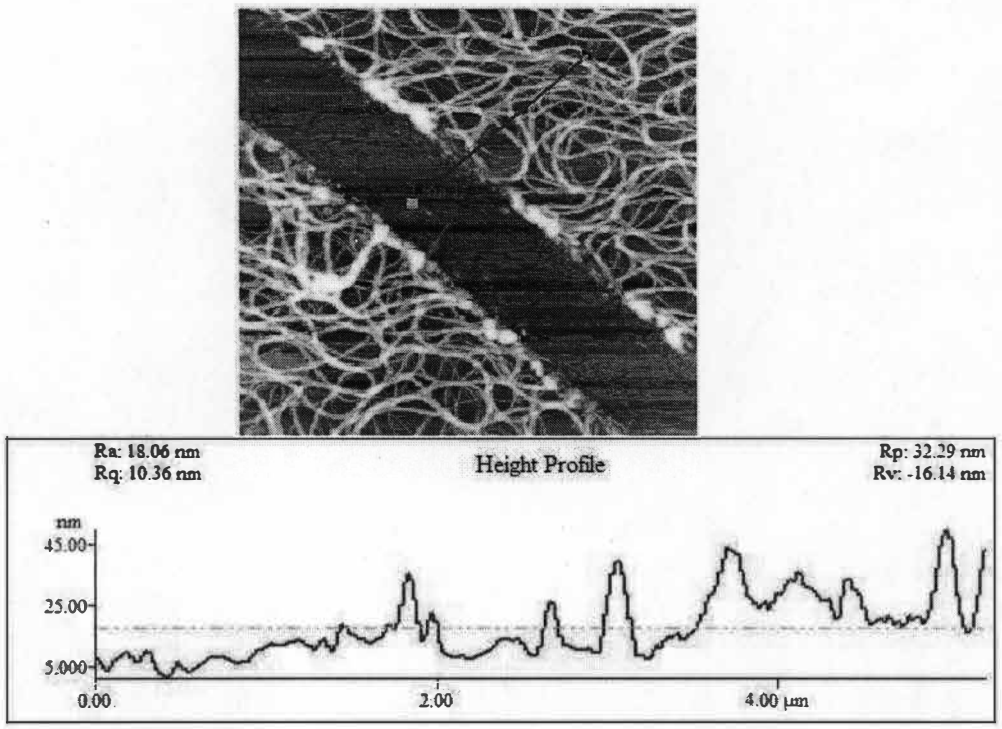

Figure 5-9. AFM micrograph and the height profile along a line depicting the average thickness of the film to be 20nm.

5.3.2. Raman spectroscopy of CNT

Raman spectroscopy is excellent analytical tool particularly for carbon nanotubes. Many properties of CNT are revealed from the Raman spectra of CNTs. Different groups have achieved atomic resolution of carbon nanotubes with Scanning Tunneling Microscopy (STM) and the structure property relation has been elucidated [6]. However, this technique is not always possible and also destructive because the nanotubes are prone to damage. Raman spectroscopy is a non-destructive method to characterize carbon nanotubes. In the current state of research, Raman spectroscopy is a reliable technique to characterize the carbon nanotubes. The Raman spectra of an individual SWNT lying on a substrate has an intense signal, which is comparable in strength to the signal from

substrate. Raman spectrum of carbon nanotubes has been used to identify the electronic behavior of a single carbon nanotube [7]. Carbon nanotubes display unique and distinct Raman spectra compared to other forms of carbon due to their one-dimensional nature [4]. Raman spectrum of single wall carbon nanotube has four prominent features. The Radial Breathing Mode (RBM) arises at a frequency ($f_{RBM} \approx 180cm^{-1}$) for which all the carbon atoms vibrate in phase and in radial direction as shown in Figure 5-10. The frequency of the radial breathing mode is directly proportional to the inverse of the diameter. The in-plane Raman active mode in graphite gives rise to the tangential G-band approximately at $1580cm^{-1}$ as shown in Figure 10. The disorders of the carbon nanotubes induce D-band at $\sim 1320cm^{-1}$ and G'-band which is the second order harmonic of D-band.

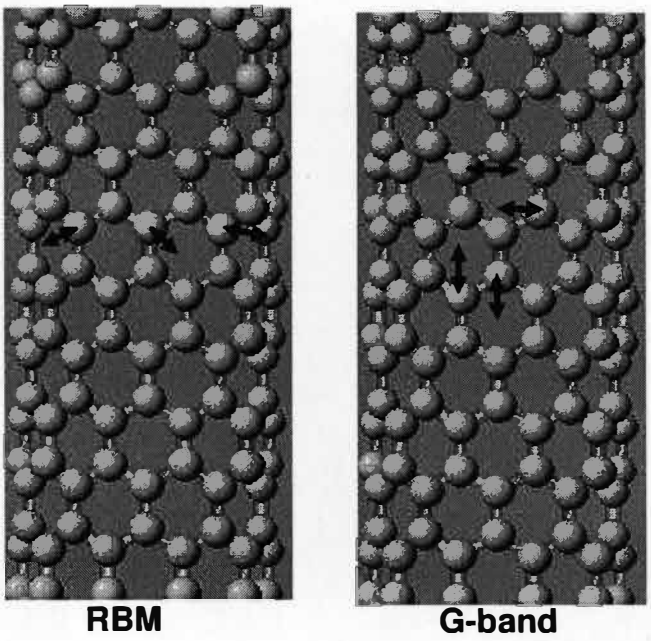

Figure 5-10. Direction of vibration of carbon atoms in (10, 0) SWNT for RBM and graphitic Raman modes.

In this work, the single wall carbon nanotubes used have been characterized by Solution 633 (Detection Inc.) Raman spectrometer. Samples were illuminated using He-Ne laser

of wave length of 633nm and energy of 1.96eV. The inherent draw back of the spectrometer used was that the start wave number was 375 cm^{-1} while the RBM of carbon nanotubes exits at ~180 cm^{-1}.

Figure 5-11 shows the Resonance Raman spectrum and Surface Enhanced Raman Spectrum (SERS) of casted nanotubes. The characteristic G-band and D-band peaks of the carbon nanotubes can be observed in both of the spectra. Resonance Raman spectra were obtained from CNTs casted on silicon substrate and so a silicon peak can be observed at approximately 550 cm^{-1}. For SERS technique, silver was thermally evaporated onto glass slides and then CNTs were casted on the thin silver film. The thickness of the silver film used was approximately 100nm.

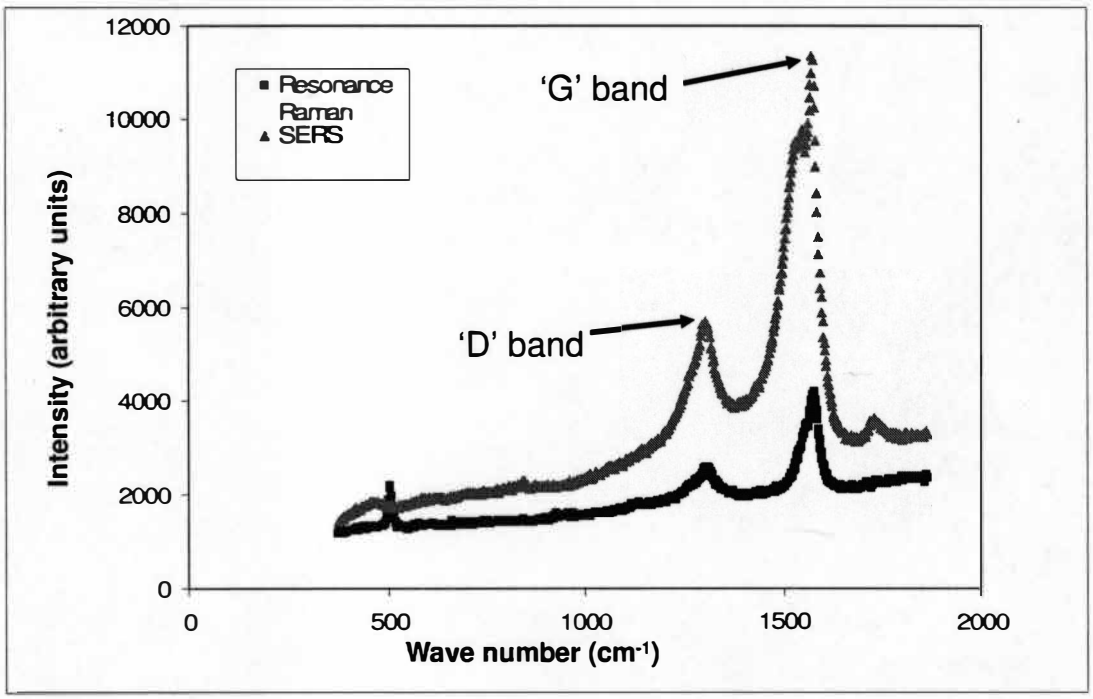

Figure 5-11. Raman spectra of CNTs obtained in resonance Raman mode and through SERS technique.

The most interesting aspect in the comparison of the spectra obtained in both the technique is the enhancement of Raman signal in the case of SERS. The G band peak intensity in the case of resonance Raman was 4196 and that in the case of SERS was 11345. The enhancement in the signal can be calculated to be 170%. It can also be observed that the silicon peak is absent in SERS spectrum because the substrate used was glass. This high enhancement in the Raman signal is desirable for the detection of carbon nanotubes in polymer and ceramic nanocomposites.

5.3.3. Electrical characterization

As discussed earlier, carbon nanotubes behave as moderate band gap semiconductors or conductors depending on chirality. In this research, all the sensors fabricated were based on CNT matrix than individual CNTs. Electrical properties of carbon nanotubes were studied using microelectrode contact pads. The electrodes were patterned by thermal evaporation of silver. A tungsten wire (Sylvania) with a diameter of 60μm was wrapped around the glass slide to mask the area of the CNTs (Figure 5-12.b). Silver was evaporated in a vacuum chamber onto the substrate on which the CNTs were casted (Figure 5-12.c). The tungsten wire mask was subsequently removed on completion of the evaporation (Figure 5-12.d).

Thus electrodes with 60μm spacing were fabricated with CNT matrix traversing between them. Figure 5-13 is optical micrographs of the silver electrodes separated by 60μm. Macroscopic probes were attached to the silver contact pads to measure the electrical properties of the matrix. After fabricating the electrodes by shadow masking technique, electrical characteristics of the matrix were studied by keithley 2700 sourcemeter which was interfaced to a computer by a LabView™ VI.

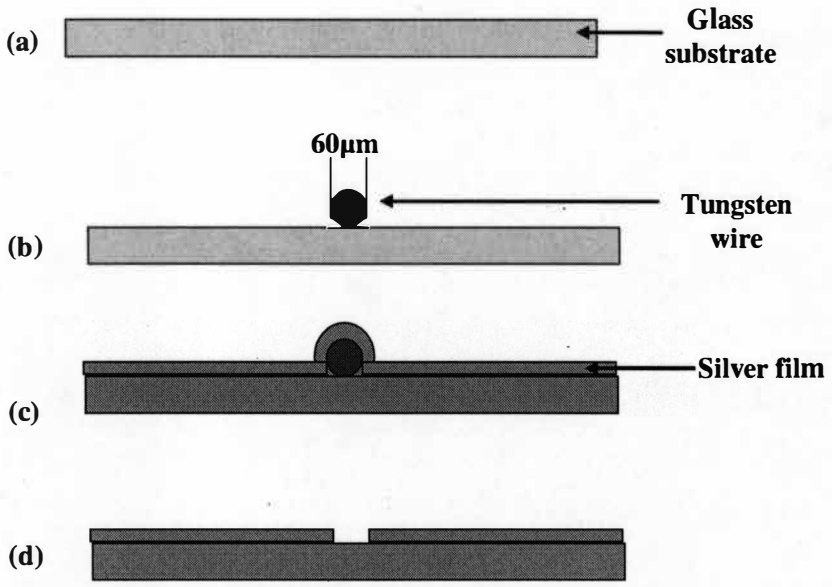

Figure 5-12. Schematic representation of the device fabrication.

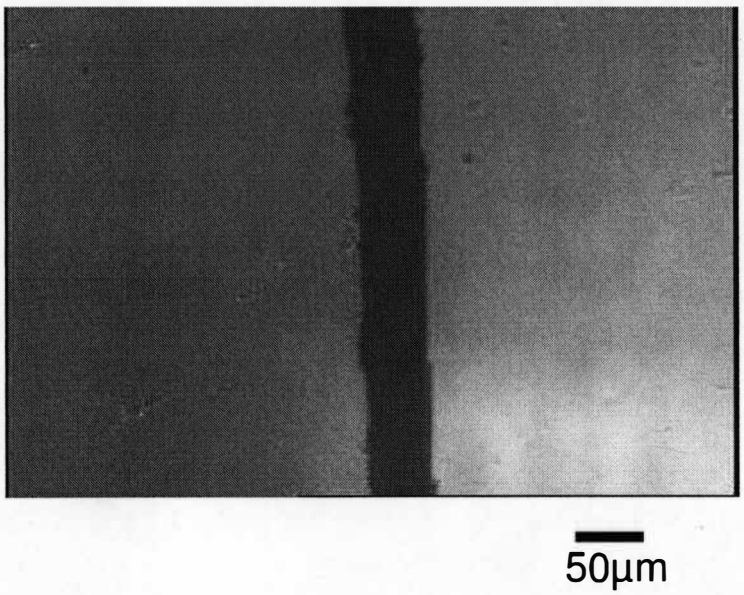

Figure 5-13. Optical micrograph of electrodes addressing the CNT matrix.

Figure 5-14 shows the I-V curve of a CNT matrix. It can be seen from the I-V curves that the matrix exhibited semiconductor properties. This is not surprising because it is well known that in a randomly selected sample of CNTs nearly 70% exhibit semiconducting behavior and the remaining 30% are metallic [6]. As it was discussed previously that SWNTs behave as metallic when n-m is divisible by 3 and behave as semiconductors otherwise. For any given n, m value, the probability of n-m being divisible by 3 is 1/3 and hence the probability of SWNT being metallic is also 1/3.

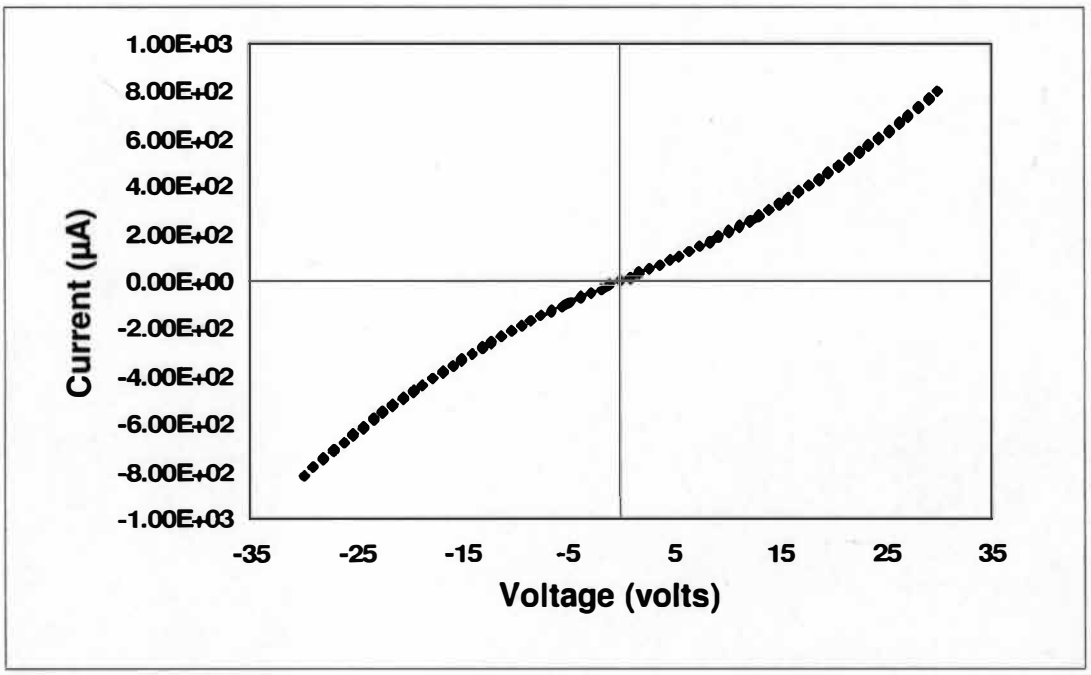

Figure 5-14. I-V characteristics of CNT matrix.

The I-V curves for low voltage scan (typically from +1V to -1V as shown in the Figure 5-15) appeared to be linear.

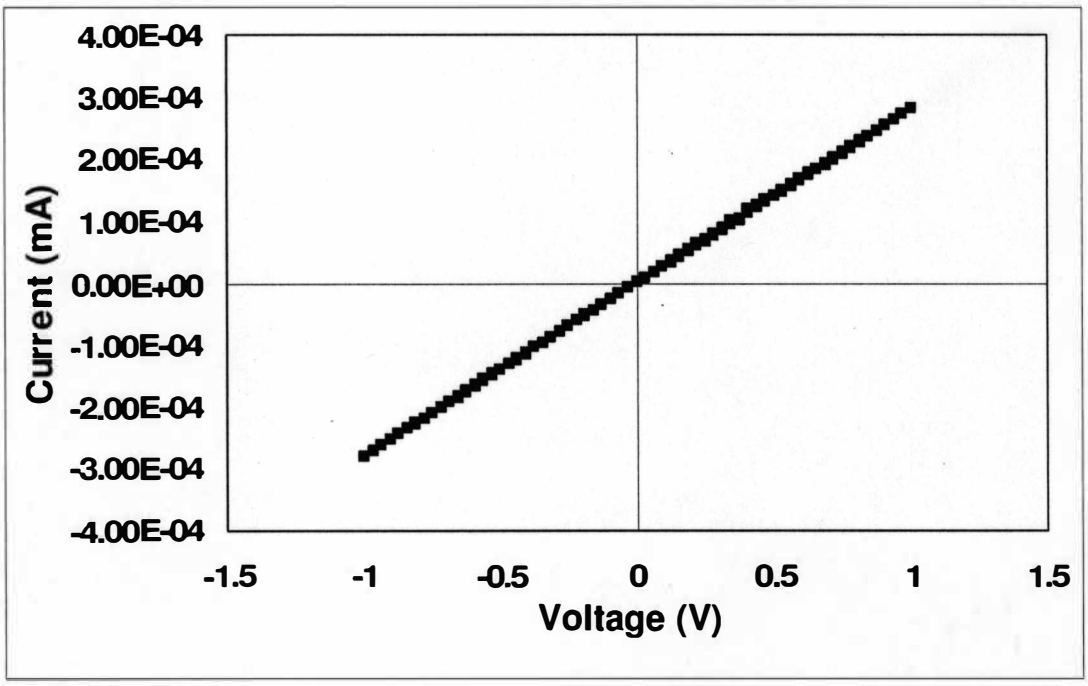

Figure 5-15. I-V characteristics of CNT matrix for small voltage range.

It is important to analyze the behavior of the matrix for such low voltages because most of the sensing experiments on the CNT matrices were performed at such low voltages. To investigate the electronic states of CNT matrices, the differential conductivity of these matrices is plotted. Differential conductivity is a plot between the ratio of differential change in the current to the differential change in the voltage to the voltage i.e. voltage (v_n) vs. $(i_{n+1} - i_n)/(v_{n+1} - v_n)$.

Figure 5-16 shows the differential conductivity for one such I-V curve for the voltage in the range of -1V and 1V. The inset shows the actual I-V curve. For electronic energy levels in a solid, density of states is defined as the number of allowed energy levels per unit volume of the solid, in the energy range E to E+dE [8] where E is any energy state. It

is known that the differential conductivity is a direct representation of the Density of States (DOS).

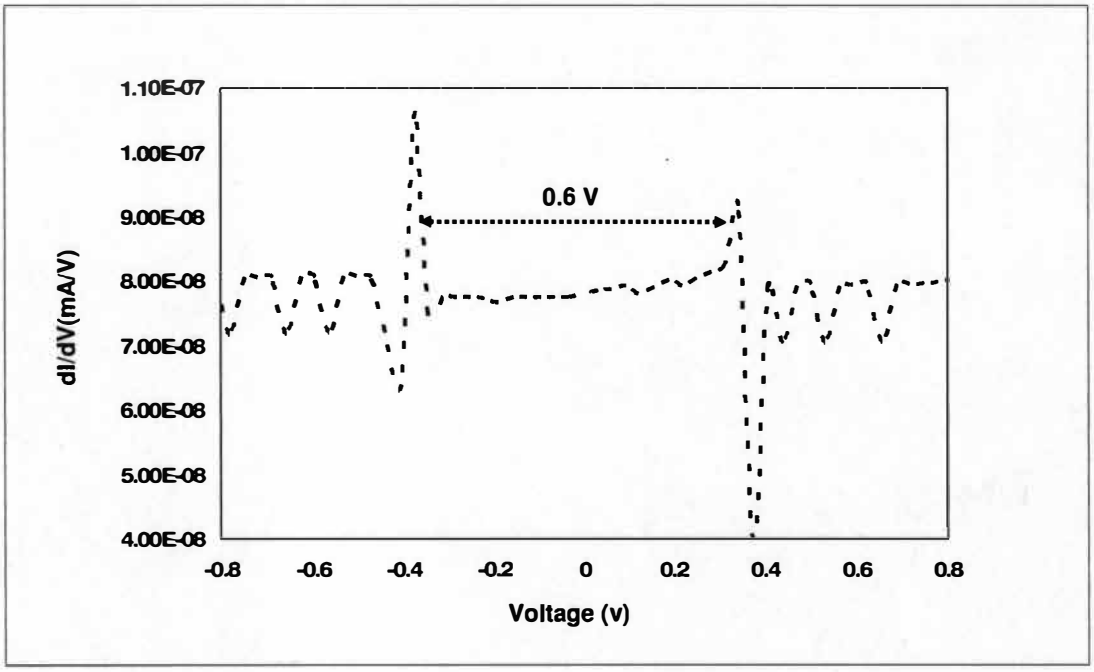

Figure 5-16. Differential conductivity of CNT matrix.

At absolute zero temperature, there are no charge carriers in the DOS at the Fermi energy and a band gap for semiconductor is about 0.6 eV. It can be seen from the plot that the gap between the first possible states of the CNT matrix is 0.6V. In the Figure 16, the finite energy carriers at the fermi level are calculated to be 7.75×10^{-8} mA/V which can be due to two factors. Firstly, the experiments were performed at room temperature and secondly due to the 30% metallic tubes present in the matrix. Due to the measured band gap of 0.6V it can be concluded that the CNT matrices exhibited dominantly semiconducting behavior.

In summary, this chapter described a simple and efficient way of purifying carbon nanotubes in solutions. This chapter also discussed the characteristics of the CNT used in this research. AFM and Raman spectroscopy revealed important properties of CNT. From the AFM imaging, the diameter of CNT was found to be 1.4nm. The electrical characterization revealed that the CNT matrices exhibited semiconducting behavior. The Raman spectrum revealed that there was a wide variety of nanotubes in the matrices formed.

5.4. References

[1] S. Iijima, and T. Ichihashi, Nature, vol. 363, p. 603, (1993).

[2] A. G. Rinzler, J. Liu, H. Dai, P. Nikolave, C. B. Hauffman, F. J. Rodriguez-Macias, P. J. Boul, A. H. Lu, D. Heymann, D. T. Colbert, R. S. Lee, J. E. Fischer, A. M. Rao, P. C. Eklund, and R. E. Smalley, Applied Physics A, vol. 67, p. 29, (1998).

[3] R. T. K. Baker, Carbon, vol. 27, p. 315, (1989).

[4] A. G. S. Filho, A. Jorio, G. G. Samsonidze, G.Dresselhaus, R. Saito, and M. S. Dresselhaus, Nanotechnology, vol. 14, p. 1130, (2003).

[5] A. M. Rao, J. Chen, E. Richter, U. Schlecht, P. C. Eklund, R. C. Haddon, U. D.Venkateswaran, Y. Kwon, and D. Tomanek, Physical Review Letters, vol. 86, p. 3895, (2001).

[6] J. W. G. Wildoer, L. C. Veneme, A. G. Rinzler, R. E. Smalley, and C. Dekker, Nature, vol. 391, p. 59, (1998).

[7] A. Jorio, R. Saito, A. H. Hauffner, C. M. Leiber, M. Hunter, T. Mc Clure, G. Dresselhaus, and M. Dresselhaus, Physics Review Letters, vol. 86, p. 1118, (2001).

[8] S. Raich, C. Thomsen, and P. Ordejon, Physical Review B, vol 65, p. 155411, (2002).

6. RAMAN SPECTROSCOPY STUDIES OF SWNT AND OTHER GRAPHITIC MATERIALS

6.1. Introduction

As discussed previously, Raman spectrum of single wall carbon nanotube has four prominent features. The Radial Breathing Mode (RBM) arises at a frequency (f_{RBM} $\approx$180cm^{-1}) for which all the carbon atoms vibrate in phase and in radial direction. The frequency of the radial breathing mode is inversely proportional to the diameter. The in-plane Raman active mode in graphite gives rise to the tangential G-band approximately at 1580cm^{-1}. The disorders of the carbon nanotubes induce D-band at ~1320cm^{-1} and G'-band which is the second order harmonic of D-band [1].

The Raman spectrum of Highly Oriented pyrolytic Graphite (HOPG) has been well established [2]. For single crystalline graphite, only one Raman line was observed at ~1575 cm^{-1} (G-band). For all other forms of graphite, one more line is observed at ~1355 cm^{-1}. The intensity of this line is directly proportional to the amount of unorganized carbon present in the sample and the decrease in the graphite crystal size. This is the same as the disorder induced band (D-band) in the case of carbon nanotube spectrum.

In this work, a comparative study of diminishing intensity and the downshift of G-band peak [3] (due to the in-plane Raman active mode of graphitic carbon) of the thin films of carbon nanotube and Highly Oriented Pyrolytic Graphite (HOPG) at elevated temperatures was performed.

6. 2. Experimental details

Raman spectrum was obtained from Solution 633(Detection Limit Inc.) Raman spectrometer. He-Ne laser of wavelength 633 nm was used as the excitation source. The energy of the laser source is 1.96eV.

The filtered solution of CNTs was ultrasonically agitated to derope the bundled carbon nanotubes. The carbon nanotubes were then casted on silicon substrates using a micropipette. The silicon substrates were cleaned before casting SWNT solution with Isopropyl Alcohol to remove any contamination on the surface.

The casted sample was mounted on a hot plate whose temperature can be varied from room temperature to 700 K. The entire set up was placed under the Raman probe and spectrum was taken. The temperature of the silicon substrate on the hot plate was measured with an optical thermometer. This method exactly provides the temperature of the substrate taking losses due to the environment into account. Temperature dependence of Raman spectrum of freshly cleaved HOPG (ZYA grade purchased from Micromasch) was studied with a similar setup.

6. 3. Results and analysis

Figure 6-1 shows the Raman spectrum of carbon nanotube and the HOPG at room temperature. The G-band and the D-band of SWNT can be seen while in the case of HOPG the D-band intensity was very weak compared to the G-band as the HOPG is relatively higher crystalline compared to the other forms of carbon like stress annealed graphite and carbon black. The HOPG used in these experiments was of ZYA grade with a mosaic spread of 0.4±0.1 and a lateral grain size of 10mm. In the case of SWNT, the

Raman spectrum also has the silicon peak (shown in the Figure 1 by *) arising from the substrate at ~550cm^{-1}. The carbon nanotube tube spectrum was obtained for elevated temperatures using a hot plate.

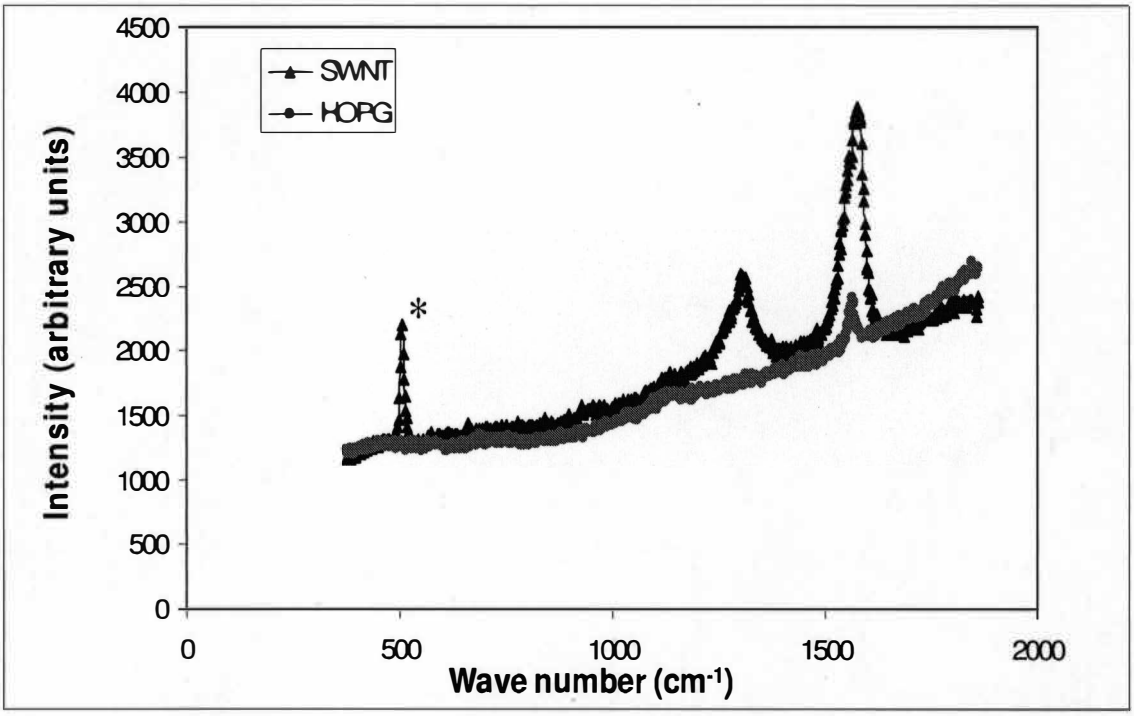

Figure 6-1. Raman spectrum of SWNT and HOPG at room temperature (* in the figure indicates silicon peak).

The Raman spectrum of carbon nanotubes at various temperatures is shown in Figure 6-2. It can be seen that there is a downward shift in the G-band peak. The G band peak of CNT plotted against the temperature showed a linear trend and the temperature coefficient of G band is calculated to be ~0.044cm^{-1}/K.

Similar experiment performed with HOPG resulted in a slightly different result. The G-band peak of the HOPG also exhibited a downward shift with the elevation of temperature but the temperature coefficient was found to be ~0.031cm^{-1}/K. Figure 6-3 shows the spectrum of HOPG at different temperatures and the inset shows the zoomed in

plot of the G band peak Vs Intensity. It can be clearly seen from the plot there was a negative shift in the peak.

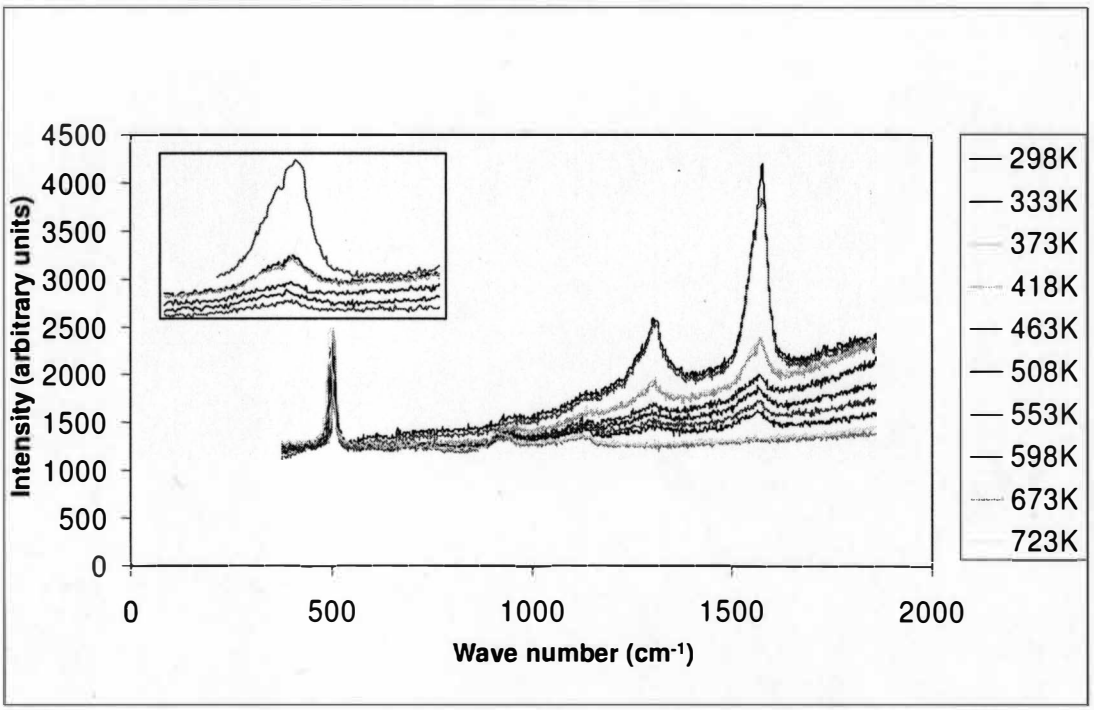

Figure 6-2. Raman spectrum of SWNT at different temperatures showing the downward shift of the G band peak and the decreasing intensity.

Figure 6-4 shows the plot between temperature and the peak wave number of the G-band for SWNT and HOPG. It can be seen that both the trends are linear with different slopes. SWNT exhibited a bigger slope compared to HOPG. The other interesting aspect observed was that there was a decrease in the intensity of the G band with elevation of temperature in the case of both SWNT and HOPG.

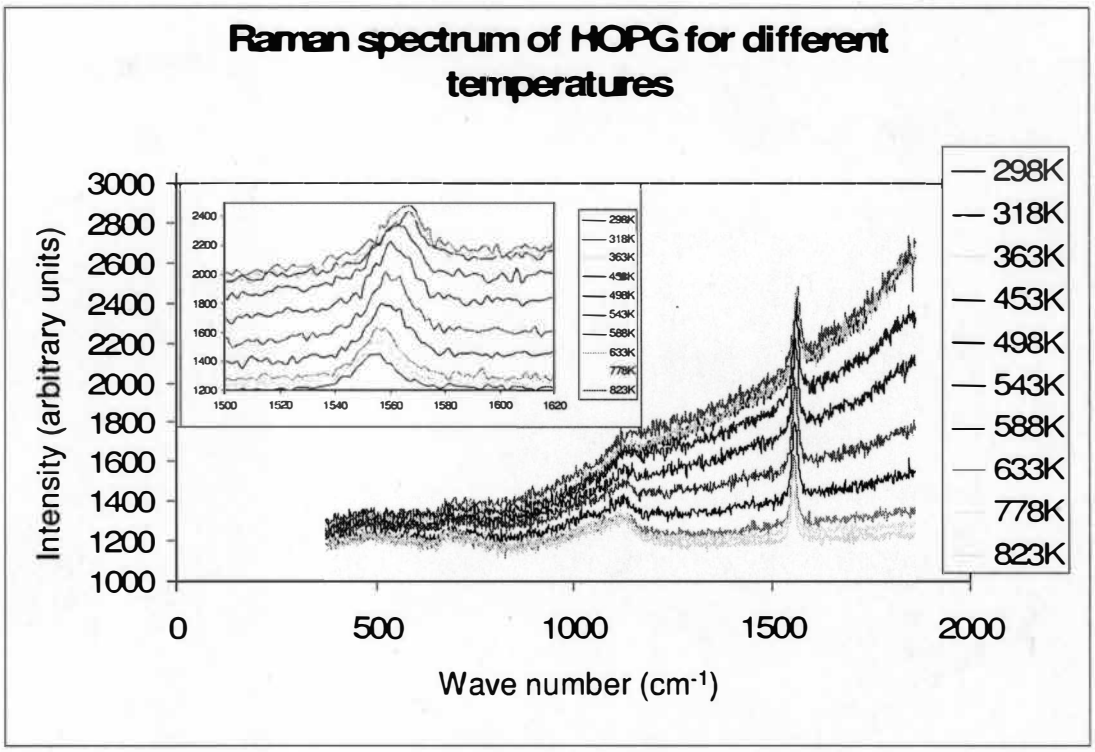

Figure 6-3. Raman spectrum of HOPG at different temperatures showing the downward shift of the G band peak and the decreasing intensity.

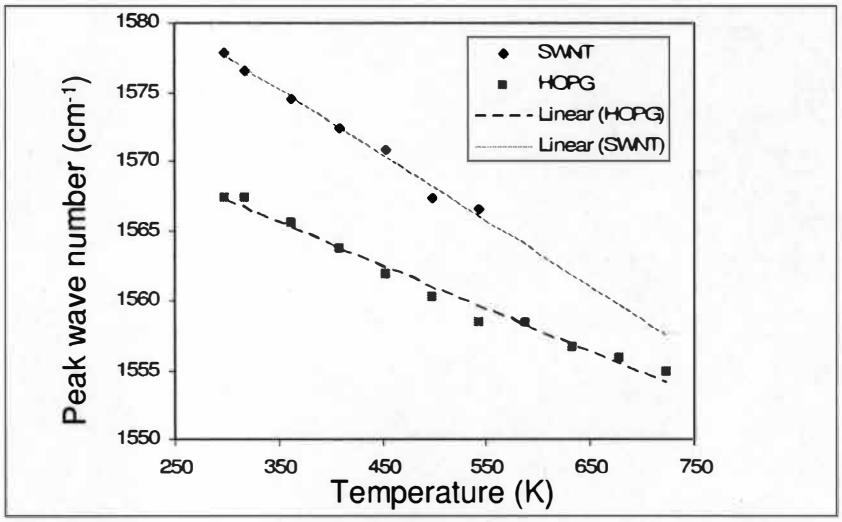

Figure 6-4. Temperature vs. G-band peak for SWNT and HOPG.

The downshift in the G-band peak in various carbonaceous materials is due to the lengthening of C-C bond [4]. The different rate of this downward shift for HOPG and SWNT might be because of the difference in their structure. HOPG has a planar structure with carbon atoms arranged in a honeycomb fashion. Such sheets of graphite are stacked one over the other. On the other hand, SWNT can be imagined as a single sheet of graphene rolled up to form seamless cylinder. The cylinder is closed at the ends by two hemispheres of buckminster fullerene molecule. At elevated temperatures, in the planar graphite sheets of HOPG, the C-C bonds elongate against the restoring force between the bonds.

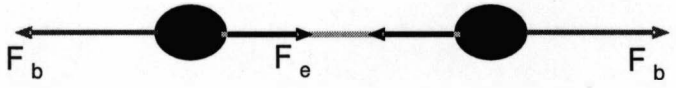

(a)

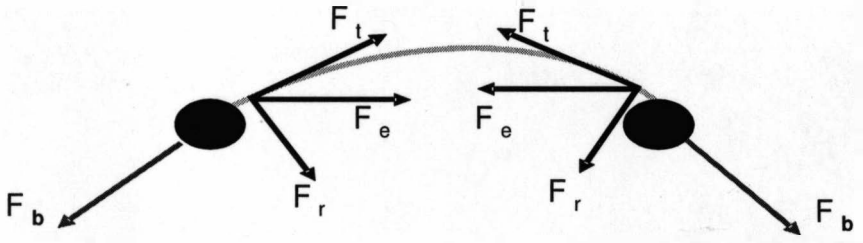

(b)

Figure 6-5. Schematic representation of C-C bond stretching in (a) HOPG (b) SWNT.

Figure 6-5(a) shows the bond stretching and the restoring forces in the planar HOPG. It can be seen that the restoring force is just acting in opposite direction to the bond stretching direction. The same restoring force does exist in the case of carbon nanotubes

but a new radial component of this force arises because of the cylindrical structure of the carbon nanotube. So the restoring force now has two components one tangential and the other radial. Figure 6-5(b) shows the curved carbon-carbon bonds. F_b is the bond stretching force because of the temperature. F_e is the restoring force which tries keeping the atoms in same position. This force has two components one in the radial direction and the other in tangential direction. The radial force helps in conserving the tubular morphology. Only the tangential component acts against the bond stretching and a part of the restoring force (radial component) is lost. So the C-C bond elongation in the case of SWNT is more compared to the planar graphite (HOPG) where the restoring force has only one component which acts in the opposite direction to bond stretching. Due to this, one can expect a higher shift in the G-band peak of SWNT for the same temperature change compared to planar HOPG.

The other interesting observation in this experiment was there was a decrease in the intensity of the signal of G-band peak as the temperature was increased in the case of both SWNT and HOPG. The decrease of intensity in the signal can be seen in Figure 6-2 and Figure 6-3 for SWNT and HOPG respectively. The plot for the intensity versus temperature is shown in Figure 6-6. There was no signal from SWNT after 700 K. This completely agrees with the fact that CNT are stable up to 700 K and start deteriorating at higher temperatures.

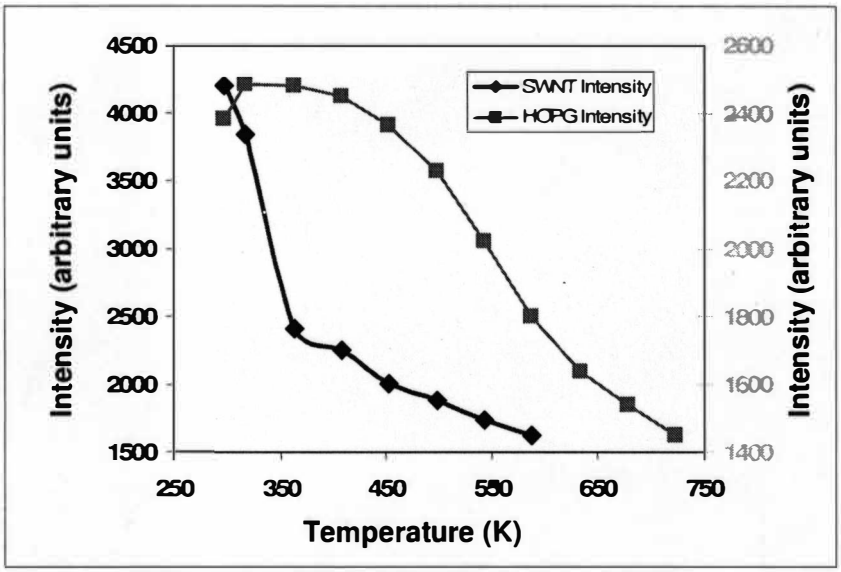

Figure 6-6. Intensity of G band vs. temperature for SWNT and HOPG.

To conclude with, the temperature dependence of Raman spectrum is carefully studied for both SWNT and HOPG. Temperature coefficient of G-band peak for SWNT and HOPG was found to be approximately -0.044cm^{-1}/K and -0.031cm^{-1}/K respectively. The author speculates variation in the temperature dependence, with SWNT having a higher magnitude of coefficient, of G-band is due to the structural difference between graphite and HOPG. A new component of the restoring force arises in the case of SWNT because of the curvature. Because of this, there is slightly weak restriction against the bond stretching and hence SWNT exhibit a higher temperature coefficient. A decrease in the intensity of the G band peak was also observed in the case of HOPG and SWNT with increasing temperature.

6.4. References

[1] A. G. S. Filho, A. Jorio, G. G. Samsonidze, G. Dresselhaus, R. Saito, and M. S. Dresselhaus, Nanotechnology, vol. 14, p. 1130, (2003).

[2] F. Tuinstra, and J. L. Koenig, Journal of Chemical Physics, vol. 53, p. 1126, (1970).

[3] N. R. Raravikar, P. Keblinski, A. M. Rao, M. S. Dresselhaus, L. S. Schadler, and P. M. Ajayan, Physical Review B, vol. 66, p. 235424, (2002).

[4] P. Tan, Y. Deng, Q. Zhao, and W. Cheng, Applied Physics Letters, vol. 74, p.1818, (1999).

7. CARBON NANOTUBE BASED BIOLOGICAL AND CHEMICAL SENSORS

7.1. Introduction to CNT based biosensors

Nanotechnology and Biotechnology are two different fields of science at the same size scale. There is an inherent relation between the two great revolutions of bio and nano technologies. Biological systems like the DNA formed the inspiration behind the creation of many novel nanostructured materials. These two fields are the most exiting facets of science, which can go hand in hand. Carbon nanotube is an interesting material at the intersection of these two technologies. Although carbon nanotubes have many applications, one of the most important and promising applications which might find a significant place in the technologies related to these buckytubes is its biosensing ability [1, 2]. The unique electronic properties of CNT in conjunction with the specific recognition properties of the incubated biomolecules would make CNTs as ideal nanoscale biosensors. A careful observation reveals that carbon nanotubes have the large surface area with all the carbon atoms on the surface. Hence, by a careful alteration of the surface chemistry of the carbon nanotube, they can be exploited for biosensing applications [3]. It has been recently demonstrated that individual semiconducting single wall carbon nanotubes can be used for the detection of glucose oxidase [4]. Controlled attachment of the glucose oxidase enzyme (GOx) to the SWNT sidewall was achieved through a linking molecule which resulted in a clear change of the conductance of the sensing device.

7.2. Sensing mechanisms

In this research two types of sensing mechanisms have been used to demonstrate the ability of carbon nanotubes to form nanoscale biosensors. The first sensing mechanism involves a CNT based conduction sensor in which the decrease in the current was observed on the binding of the specific biomolecule. In the second mechanism Quartz Crystal Microbalance (QCM) was used to quantify the mass of the biomolecule bound on the sidewalls of the carbon nanotube. Both the sensing mechanisms proved to be efficient and consistent.

7.3. Conduction based sensor

The purified carbon nanotube solutions were sonicated and then the solutions were casted on glass substrates. Before casting with the solutions, the glass substrates were cleaned in Isopropyl alcohol bath and dried in a conventional oven. The microelectrode contact pads had to be formed across the network of CNTs on the glass substrate. Silver was thermally evaporated using shadow masking technique to form the gap between the electrodes. A 60μm tungsten wire was wrapped around the area where CNTs were present. After the evaporation was complete the tungsten wire was removed leaving CNT with electrodes across them. Figure 7-1 shows the schematic of the fabricated sensor.

7.4. CNT based QCM sensor

QCM experiments were performed using 5 MHz AT-cut Quartz crystals coated with carbon nanotubes. SWNT were casted on the gold surface of the quartz crystal. Then the chip was baked at 50° C for one hour. The presence of the CNT on the gold surface was confirmed by Raman spectroscopy. Figure 7-2 shows the Raman spectrum of CNT on

the gold surface. The characteristic G-band and D-band peaks of the carbon nanotube can be observed.

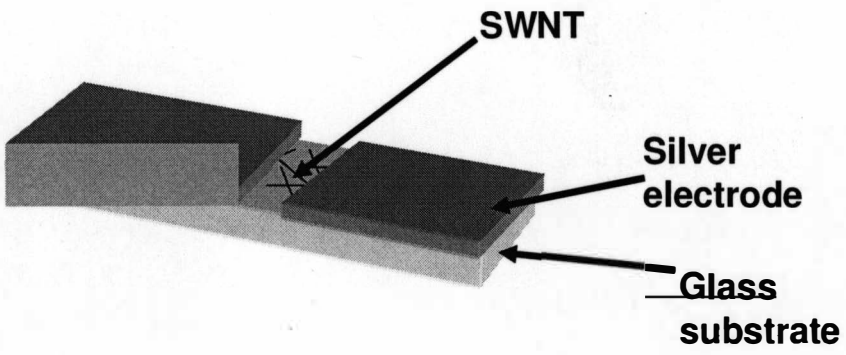

Figure 7-1. Schematic of the fabricated conduction based sensor.

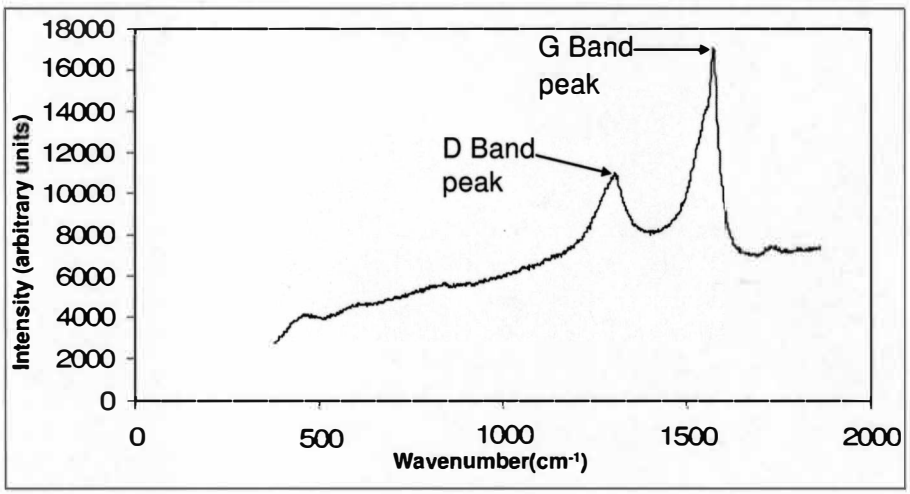

Figure 7-2. Raman spectrum of gold surface of QCM casted with SWNT.

7.5. Experimental details

Agilent multimeter (Agilent-3458A) was employed to monitor the electrical changes of the CNT matrix which was interfaced with a computer. A constant voltage was applied

between the electrodes and the conductance changes for various concentrations of the protein and antibody were recorded. Protein solutions were added to 10 µl of PBS that had been placed on the sensor. PBS was employed as a buffer environment to distinguish changes in CNT matrix conductivity due to protein binding as shown in Figure 7-3.

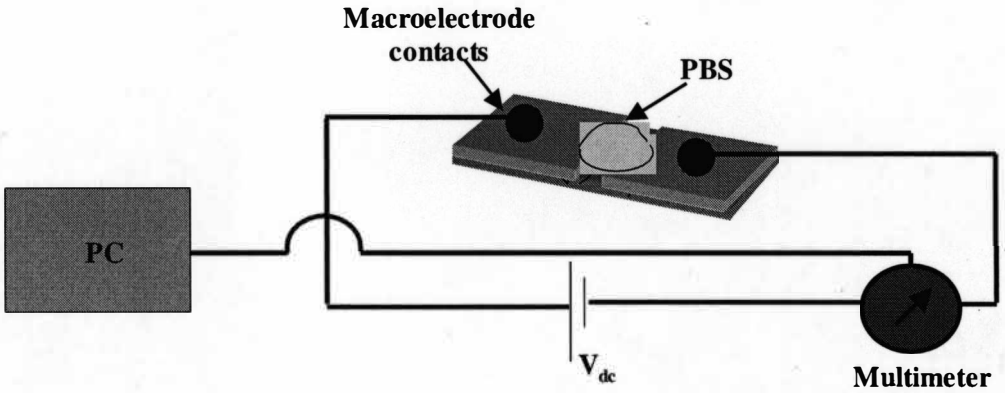

Figure 7-3. Schematic representation of the sensor with the PBS on the CNT.

Measurements of CNT coated QCM crystals were performed by covering the chips with PBS before addition of the protein solutions. Approximately 200 µl of PBS was used to cover the entire chip. QCM is highly sensitive to viscosity. In order to avoid change in frequency due to viscosity changes, the chip was covered with PBS and then protein solutions (of the same viscosity) were added to adjust the concentration to desired levels.

7.6. Sensor responses

Five microliters of a solution of Streptavidin with different concentrations was added to the 10µl of PBS on the sensor to result in 10nM, 1µM and 2µM of protein. Figure 7-4 shows the electrical response of the sensor to different protein concentrations. Point 1 indicates the instance at which 10µl of PBS was introduced between the electrodes and

point 2 is the time at which 5µl streptavidin solution was added to the PBS making the final concentration of the protein to be 10nM. It can be seen that there was no appreciable change in the current. The protein concentration was increased to 1µM at Point 3 and a decrease in the conductance of the CNT matrix was observed. The current decreased from 97.7µA to 60.3µA which corresponds to approximately a 40% change in conductance. After the current stabilized, the protein concentration was further increased to 2µM and a further decrease in current was recorded. The change in conductance was 17.5% (60.3µA to 49.7 µA), which is smaller compared to the initial change. The smaller change in the conductance can be attributed to fewer active sites available for the second group of protein molecules to bind to CNT.

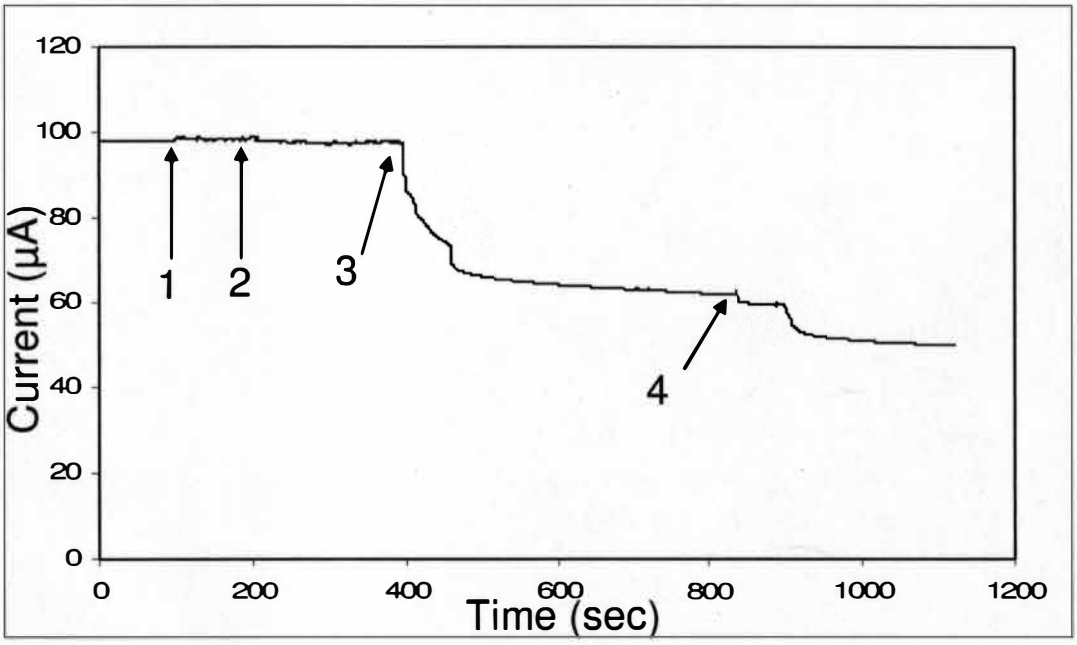

Figure 7-4. Electrical response of sensor for various concentrations of streptavidin.

Figure 7-5 is an AFM micrograph of the CNT and protein molecules. From this Figure, it

can be seen that protein molecules were bound on the sidewalls of the tube and bundles of CNT were decorated with Steptravidin molecules.

Figure 7-5. Streptavidin molecules decorating the SWNT side walls.

The imaging was performed with a very low concentration of streptavidin (1nM). Images with concentration of 10μM revealed complete protein coverage on the sample as shown in Figure 7-6.

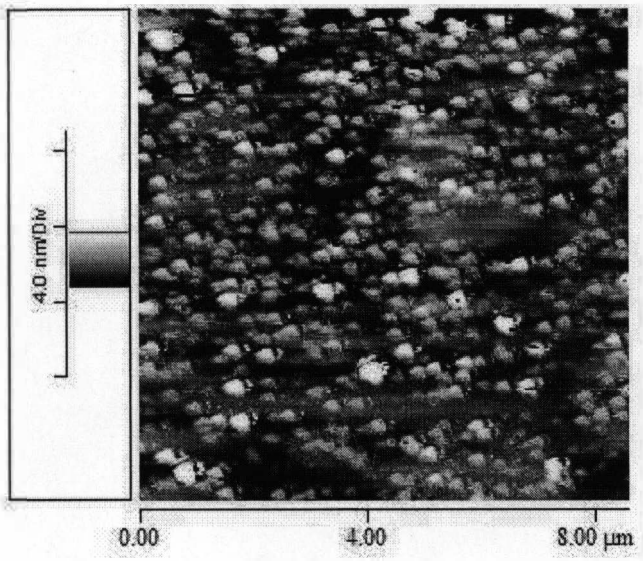

Figure 7-6. 10μM concentration of streptavidin resulting in a complete coverage on the sample.

Figure 7-7 shows the sensor response to the mouse monoclonal IgG. Following introduction of PBS and 1μM of IgG, the current decreased from 71.2μA to 45.4μA,

which is nearly a 36% change in conductance. With increase of concentration to 2μM, the current further decreased to 30μA, which is a 30% change. This is consistent with Streptavidin behavior, which can be attributed to fewer active sites available for binding of IgG to CNT.

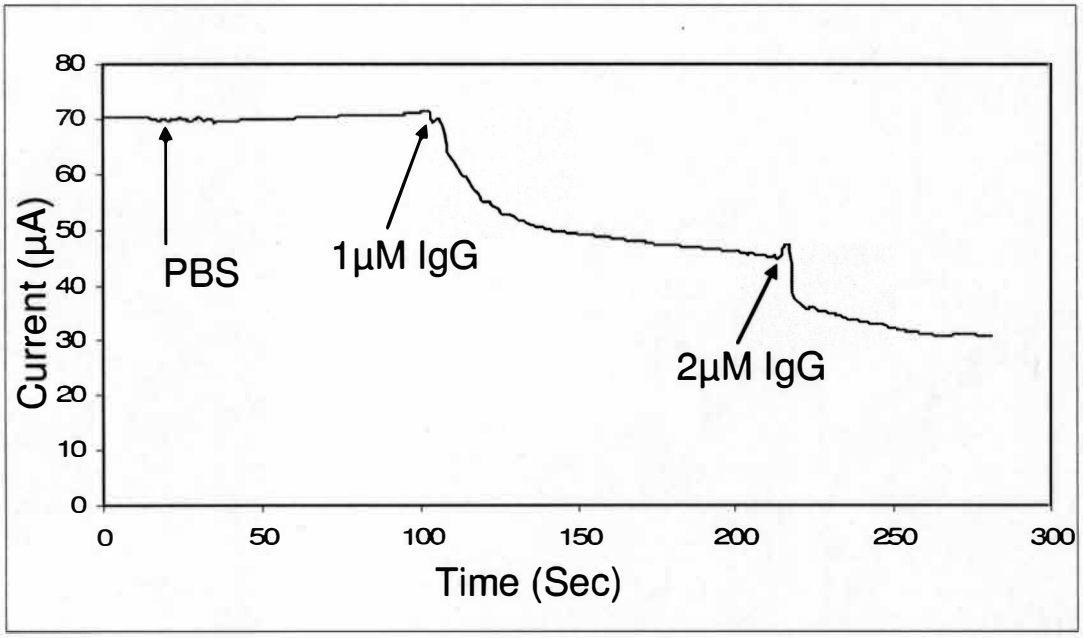

Figure 7-7. Electrical response of sensor for various concentrations of IgG.

The concentration of the biomolecule forms the "control" for the fine modulation of current between the electrodes. The spontaneous adsorption of both the biomolecules on the surface of carbon nanotube can be because of the hydrophobic interaction. The change in the conductance can be explained in a simple way. Streptavidin is a tetrameric protein which binds very tightly to the small molecule, biotin. It has molecular weight of 64 KDa according to the dielectrophoretic measurements. It is known from previous studies that streptavidin is electrically neutral at a pH between 6 and 7.2 [5]. However, the surface of the protein molecule still consists of strong residual bases. These bases are

responsible for charge transfer. The charge transfer in the case of IgG can be explained in a similar way.

The quantitative study of mass uptake of CNT network due to biomolecules immobilization was performed using QCM. In QCM, a chemical interface on the surface of the sensor selectively adsorbs materials in the solvent to the surface of the sensing area. In our context, the chemical interface is the CNT matrix on the gold surface coated on the QCM crystal. Measurements of CNT coated QCM crystals were performed by covering the chips with PBS before addition of the protein solutions. Figure 7-8 depicts the QCM response using streptavidin. For a concentration of 1μM of streptavidin, a change of 120 Hz in resonant frequency was recorded. From the Sauerbrey equation the mass bound was calculated to be 1.538μg. when the concentration on the chip was increased to 2μM, the change in the frequency was found to be 26Hz. This corresponds to a mass uptake of 0.33μg.

The lower frequency shift can be attributed to fewer active sites available for the protein molecules as described in the conductance based sensors.

Similar experiments were performed with IgG and the frequency change was 248Hz using a 2 μM concentration. Figure 7-9 shows the QCM response for the IgG incubation. When the crystal was resonating at its natural frequency, the carbon nanotube solution was introduced on to the chip. After the chloroform evaporated, the frequency stabilized and the CNT formed a uniform matrix on the surface.

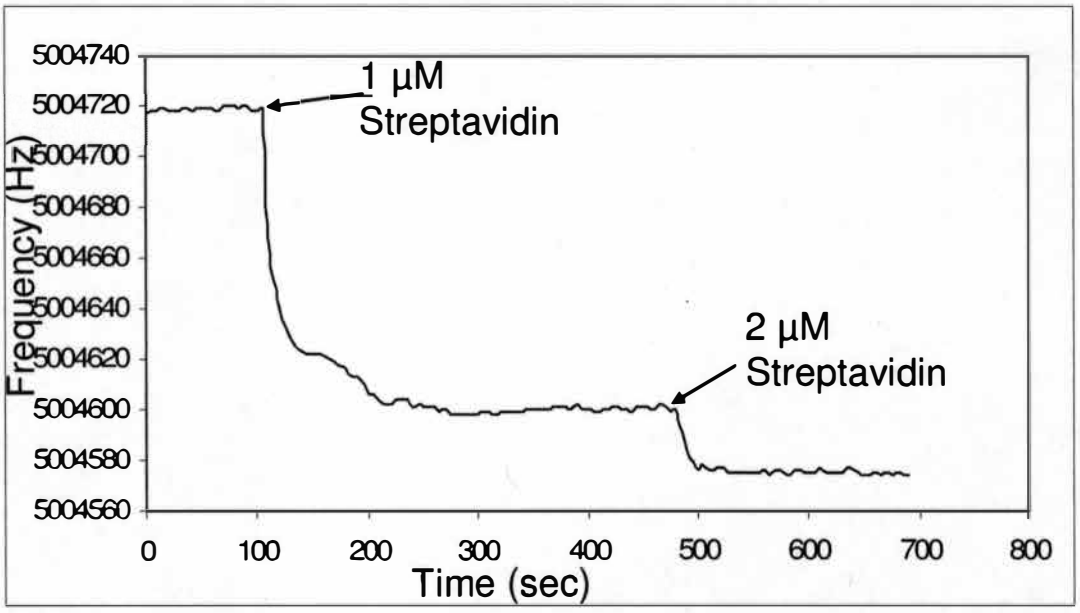

Figure 7-8. QCM response for various concentrations of streptavidin.

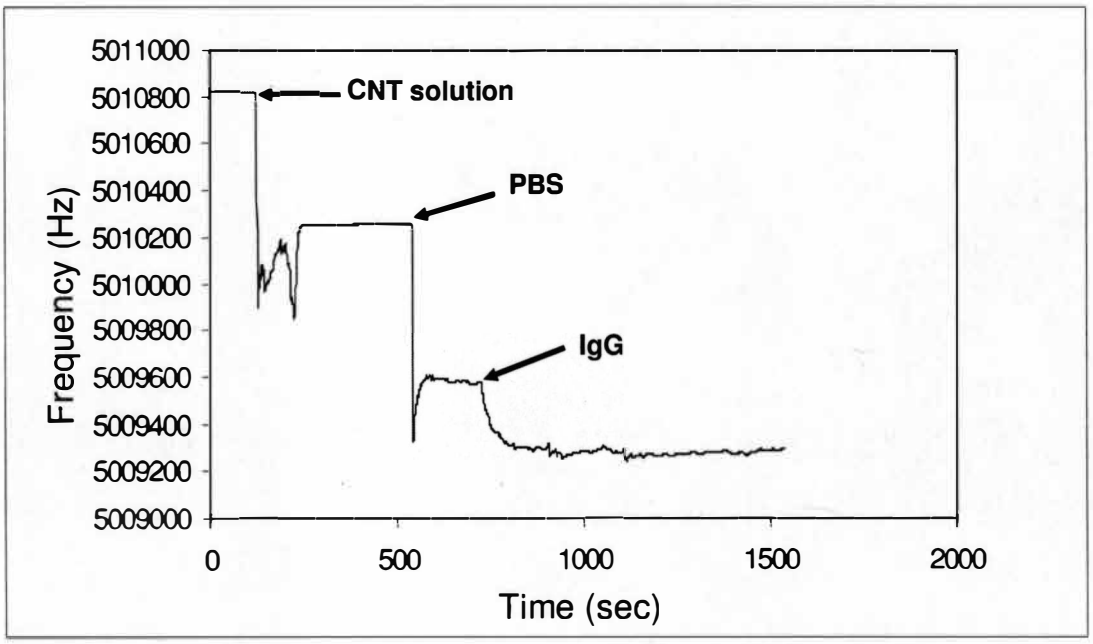

Figure 7-9. QCM response for various concentrations of IgG.

Then PBS was introduced on to the chip and due to change in the viscosity a frequency shift was recorded. After the frequency stabilized, finally the IgG antibody was introduced and the frequency change of 248 Hz was recorded for a concentration of 2 μM. This frequency corresponds to mass of 3.17 μg.

Table 1. Response of conduction based sensor and QCM for different concentrations of streptavidin and IgG.

	Streptavidin		Mouse monoclonal IgG	
	1μM	2μM	1μM	2μM
Electrical response	37.4 μA	10.6μA	25.8 μA	15.4 μA
QCM response	120Hz (1.53μg)	26Hz (0.33μg)	192Hz (2.46μg)	56Hz (0.71μg)

In conclusion, this chapter dealt with biological sensing applications of carbon nanotubes. The biomolecules were adsorbed on the sidewalls of carbon nanotube. The adsorption of the biomolecules resulted in a significant decrease in the conductivity of the matrix. The mass of the biomolecule bound was quantitatively analyzed using QCM. The summary of the responses of various sensors is given in the Table 1. Carbon nanotube may find significant applications in the new generation of biosensors. Functionalization of carbon nanotube might significantly improve the chemical compatibility and selectivity of the

sensors [1].

7.7. Introduction to chemical sensors

Highly accurate, miniature gas sensors are critical to environmental monitoring, control of chemical processes, space missions, and agricultural and medical applications [6]. The detection of nitric oxide, for instance, is important to monitoring environmental pollution resulting from combustion or automotive emissions. Detection of ammonia is required in industrial, medical, and living environments [7]. The recent experimental and theoretical studies show that the transport and electronic properties of single walled carbon nanotubes might significantly change upon exposure to gas such as O_2, NO_2 and NH_3 [8]. This new finding about SWNTs is of great importance in practical applications of nanotubes. The brighter side of this is that it could help the development of better gas sensors which are highly sensitive and extremely small. On the other hand, the performances of novel nanotube based electronic devices may be dependent on the atmospheric environment. Especially, the presence of gasses to which SWNT properties are sensitive might significantly affect the performance of new generation electronic devices based on nanotubes.

The mechanism for a high change in the transport properties of carbon nanotubes was theoretically studied by many groups [9]. From these studies, it was concluded that the nanotubes had small binding energies with NO_2 and NH_3 molecules indicating that these molecules undergo physical adsorption, and not chemical adsorption. It was also discovered that there was a charge transfer between the adsorbed gas molecules and the SWNTs. However, this charge transfer depends on the nature of the gas adsorbed. For example, for the charge transfer between the adsorbed molecule and CNT is in opposite

ways for the (NO_2) and (NH_3) gases, with electron charge transfer from CNT to NO_2 and electron charge transfer from NH_3 to CNT. This charge transfer directly affects the hole population of the CNT changing its conductance. In the case of NH_3, the conductance of SWNT decreases because electrons transferred from the adsorbed gas molecules nullify a fraction of the holes (charge carriers) in CNT. The conductance increases in the case of NO_2 because of the opposite effect.

In this work, SWNTs response to alcoholic vapors was studied. The CNT exhibited a sensitive and repeatable response to ethanol and Isopropyl alcohol.

7.8. Experimental setup

The conductance based sensors were fabricated in the same way as described previously in the same manner as described in the Section 7.3. The sensors prepared in this way were placed in-side a sealed aluminum chamber with the necessary electrical connections inside. The chamber also had a gas inlet and outlet. The block diagram of the sensing setup is shown in Figure 7-10. A gas flow controller (MKS 647C) was used to regulate the flow of gas into the chamber with desired flow rate. A program was developed in LabView to interface Agilent-3458A multimeter to monitor and record the changes in the electrical properties of the sensor. A constant DC voltage was applied across the macroelectrodes attached sensor and the change in the electrical current was recorded.

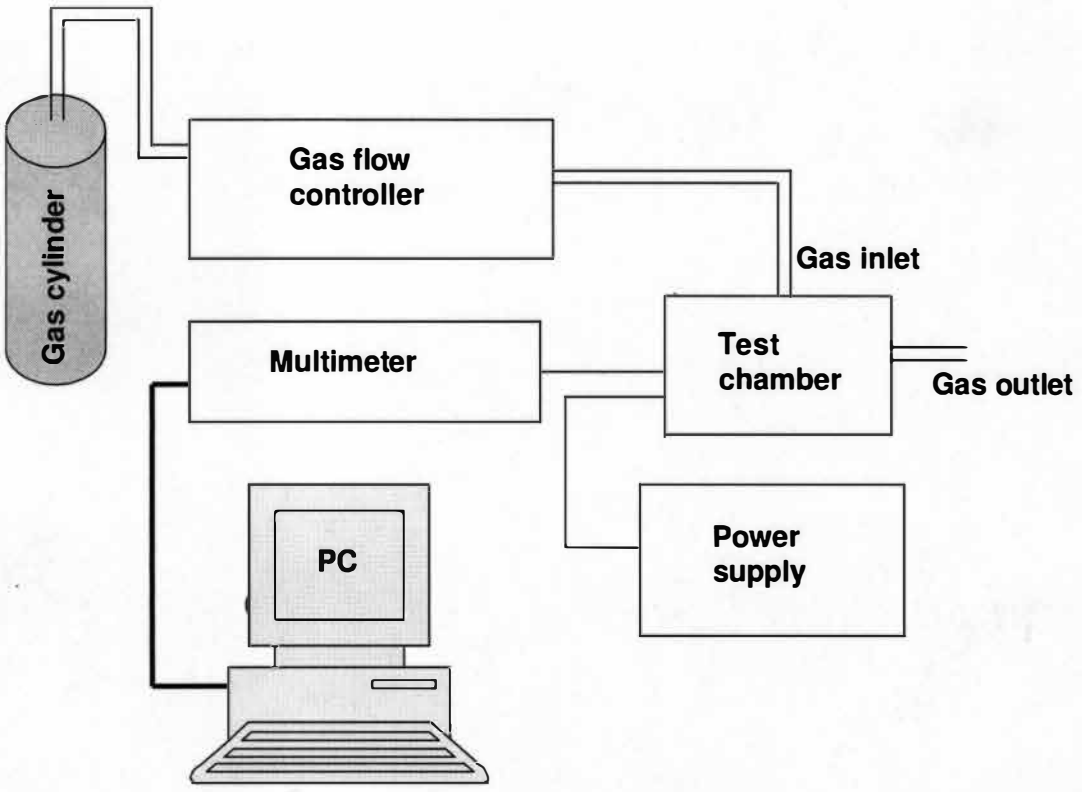

Figure 7-10. Experimental setup for chemical sensing.

7.9. Sensor response to alcohol vapors

The sensor was tested for its performance in detecting two types of alcohols

1. Ethyl alcohol (C_2H_5OH).
2. Isopropyl alcohol ($CH_3CHOHCH_3$).

The sensor exhibited a stable and consistent response for both the types of alcohols. Figure 7-11 shows the sensor response to ethanol at room temperature. Initially when the sensor was exposed ethanol a decrease in the current from 85μA to 64 μA was recorded. When ethanol was removed and the chamber was aerated the current increased to 77 μA.

Full recovery of current did not occur which might be because some alcohol molecules which were bound to the CNT surface are not detached. For further cycles of ethanol and air the sensor responses were stable with the current varying between ~77 μA and 65 μA.

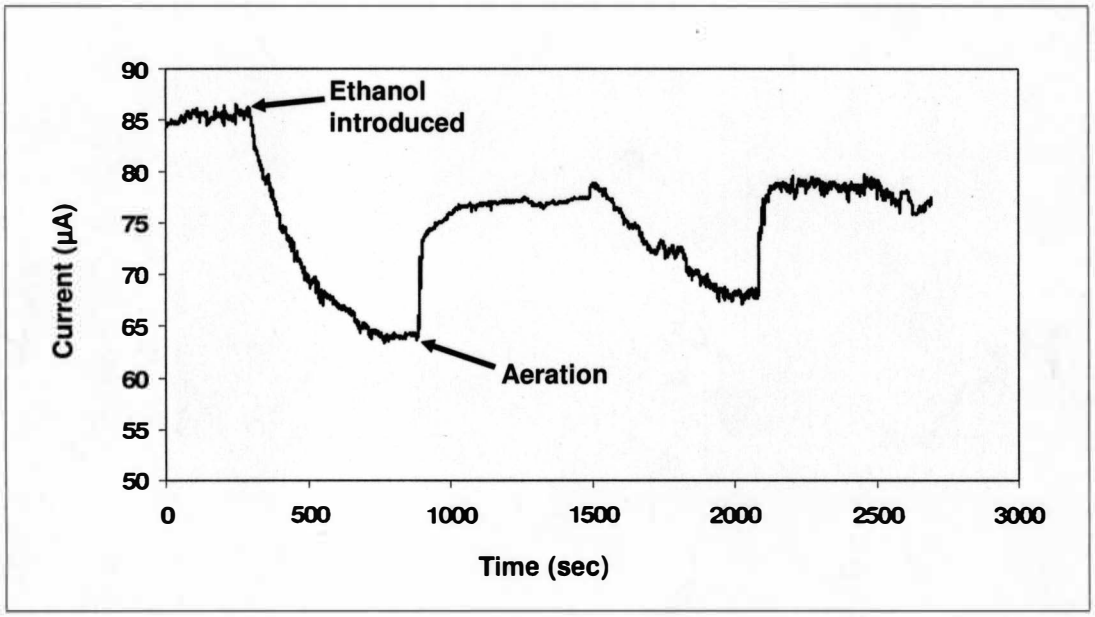

Figure 7-11. Sensor response to ethanol with the initial curing response.

Figure 7-12 shows the sensor response to Isopropyl alcohol (IPA). Initially when the sensor was exposed IPA a decrease in the current from 15.5μA to 12.5 μA was observed. Removal of IPA and aeration did not result in complete recovery. The current increased to 14.1μA. This can be considered as a curing response similar to ethanol response. For further cycles of IPA and air the sensor showed stable response between 14.1μA and 12.5μA.

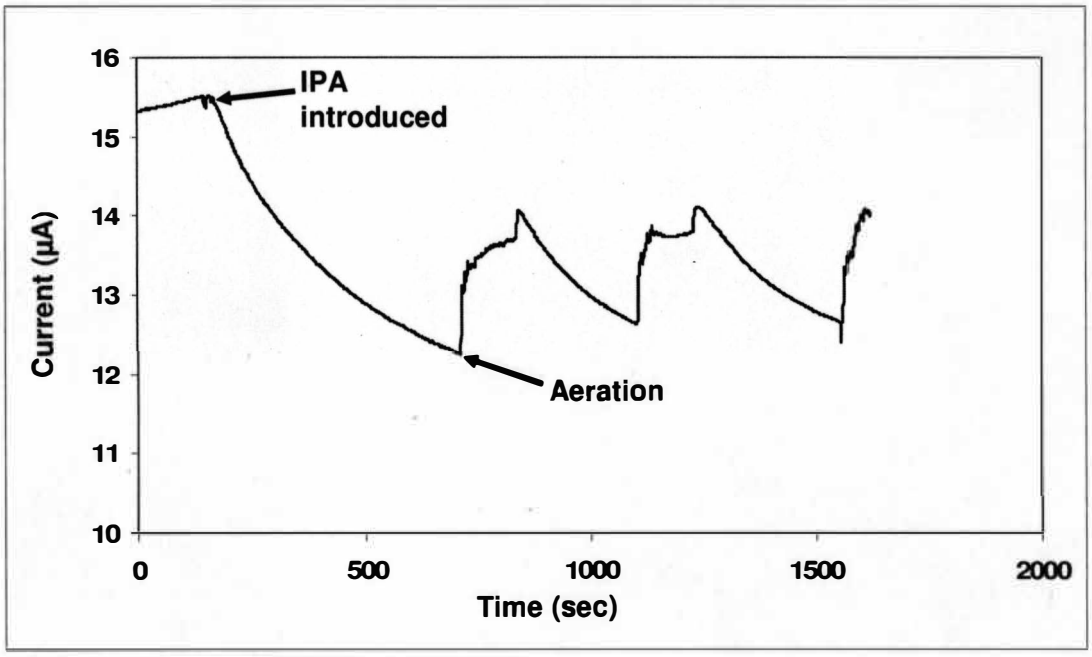

Figure 7-12. Sensor response to Isopropyl alcohol with the initial curing response.

The above two responses show that SWNT conduction is highly sensitive to alcohol vapors like ethanol and IPA. However, more precise experiments will be required to quantify the sensor performance at various concentrations of alcohol and the variations in response to different alcohols. The change in the conductance of SWNT matrix might be due to various reasons like the charge transfer between the physically adsorbed molecules on the SWNT walls or due to the alteration of Schottky barrier at the nanotube-metal interface indirectly by changing the doping level or due to the doping of the substrate. To completely understand these effects, experiments are to be designed which can individually address each of these issues.

7.10. References

[1] R. J. Chen, S. Bangsaruntip, K. A. Drouvalakis, N. W. ShiKam, M. Shim, Y. Li, W. Kim, E. J. Utz, and H. Dai, PNAS, vol. 100, p. 4984, (2003).

[2] Y. Lin, F. Lu, Y. Tu, and Z. Ren, Nanoletters, vol. 4, p. 191, (2004).

[3] R. J. Chen, H. C. Choi, S. Bangsaruntip, E. Yenilmez, X. Tang, Q. Wang, Y. L. Chang, and H. Dai, Journal of American Chemical Society, vol. 126, p. 1563, (2004).

[4] K. Besteman, J. O. Lee, F. G. N. Wiertz, H. A. Heering, and C. Dekker, Nanoletters, vol. 3, p. 727, (2003).

[5] C. J. Vanoss, R. F. Giese, P. M. Bronson, A. Docoslis, T. Edwards, and W. T. Ruyechan, Colloids and Surface B, vol. 30, p.25, (2003).

[6] Special issue on Gas-Sensing Materials, MRS Bull, vol. 24, (1999).

[7] Y. Takao, K. Miyazaki, Y. Shimizu, and M. Egashira, Journal of Electrochemical Society, vol. 141, p. 1028, (1994).

[8] J. Kong, N. R. Franklin, C. Zhou, M. G. Chapline, S. Peng, K. Cho and H. Dai, Science, vol. 287, p. 622, (2000).

[9] H. Chang, J. D. Lee, S. M. Lee, and Y. H. Lee, Applied Physics Letters, vol. 79, p. 3863, (2001).

8. FUNCTIONALIZATION OF CARBON NANOTUBES

8.1. Introduction

Carbon nanotubes have a high similarity in their chemical reactivity to graphite and other molecules of fullerene family like C_{60}. Singe wall Carbon nanotubes have extremely large surface area with all the carbon atoms on the surface. However, it is important to know that the chemistry of the nanotubes is slightly different from the other polyaromatic carbonaceous materials because of their small size, unique shape and structure. The chemical reactivity of polyaromatic carbon materials mainly arises from its dangling bonds. A perfect SWNT doesn't have any dangling bonds. However because of the curvature of SWNT the sp^2 bonds are no more planar as in the case of graphite but have a finite percentage of sp^3 hybridization. Because of this the carbon nanotubes are slightly more reactive than perfect graphite. The chemical reactivity of SWNT mainly arises from its caps since they contain six pentagons which are not found on the sidewall of the tube. The low reactivity of the sidewalls of SWNT seriously inhibits the application of nanotubes. To overcome this chemical functional groups are required on the nanotube surface which can significantly increase the reactivity and the potential applications of the tubes.

8.2. Types of functionalization

Based on the chemical reactivity of carbon nanotubes the functionalization reactions can be classified into two types. The first type of functionalization involves chemical oxidation of carbon nanotubes resulting in carboxylic, carbonyl, or hydroxyl groups. The

second type is the further functionalization of basic groups attached on the surface with some special biomolecules or other molecules sensitive to particular chemicals [1].

The other important way to functionalize nanotubes is the non covalent functionalization. This can be done by wrapping the nanotube with polymer which allows the solubility in aqueous solution [2]. The solubility of SWNT in aqueous solution can be dramatically improved by functionalization. It also preserves the nanotube structural properties and at the same time improves the processing abilities. SWNT have also been functionalized with metal particles with special properties. For example carbon nanotubes decorated with Pd nanoparticles (Pd is known to absorb hydrogen like a sponge) were formed a highly sensitive sensor for hydrogen. The H_2 absorbed by the Pd particles resulted in an electro transfer to the nanotube resulting in a decrease of conductance of SWNT [3].

8.3. Functionalization of carbon nanotubes

In order to improve the functionalization of Carbon nanotubes in water they were functionalized using various surfactants [4, 5]. When the hydrophobic part of the amphiphilic molecule contains an aromatic group, a strong interaction results, forming effective π-π-stacking with the graphitic sidewalls of the SWNT. It is believed that the nanotubes are in the hydrophobic interiors of the corresponding micelles, which results in stable dispersions.

8.3.1. Various surfactants studied

In this work we have explored the improvement of the solubility of SWNT in water by various surfactants like SDS, Tween 20, IGEPAL CA630 and Trinton X-100. All the surfactants were purchased from Sigma-Aldrich Company. 1% w/v of SWNT was

dissolved in 1% v/v solutions of various surfactants in DI water. A brief description of each of the surfactant used is given.

1. Sodium Dodecyl Sulfate (SDS): SDS ($C_{12}H_{25}OSO_3Na$) is an ionic detergent that is commonly found in household products such as shampoos. The molecule has a tail of 12 carbon atoms, attached to a sulfate group, giving the molecule the amphiphilic properties desired of a detergent.

2. Tween20: The chemical formula for Tween 20 is $C_{58}H_{114}O_2$. It is a Non-ionic surfactant that effectively suppresses unspecific reactions between anti bodies, antigens and other molecules [6]. It is also used as a solubilizer in membrane chemistry [7]. This is particular property is the motivation behind the choice of this particular surfactant.

3. IGEPAL CA630: The chemical formula of this surfactant is $C_{18}H_{30}O_3$. This is also a non-ionic surfactant.

4. Triton-100: The chemical formula of this non-ionic surfactant is $C_{14}H_{22}O(C_2H_4O)_n$ where the average value of n=9-10. This surfactant is often used as an aid for dissolution of protease in water. It is a very good wetting agent. Although IGEPAL and Triton are chemically similar to some extent triton is slightly more hydrophobic than IGEPAL.

8.4. Results and discussions

After preparation, the solutions were sonicated for 2 hours and then they were visually inspected for understanding the improvement in the solubility due to the particular surfactant. Figure 8-1 shows the photograph of the vials of solutions with various

surfactants taken after 10 min of sonification. The order of the vials from left to right is as follows: Triton-100, SDS, DI water, Tween 20, and IGEPAL CA 630.

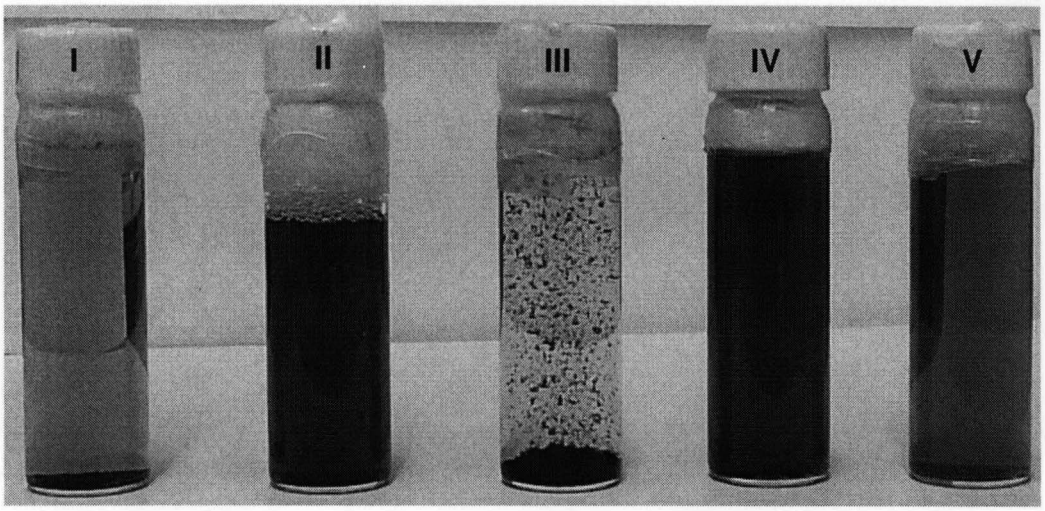

Figure 8-1. Solutions of various surfactants 10 min after sonification (I) Triton-100 (II) SDS (III) DI water (IV) Tween 20 (V) IGEPAL CA 630.

It can be seen from the picture that SWNT are least soluble in water. Within 10 minutes after sonification they exhibit the tendency to settle at the bottom of the vial. It can also be observed from the figure that Triton treated tubes also showed poor dispersion. Black soot can be observed at the bottom of the vial which is the SWNT settling at the bottom. The remaining solutions had a darker tint compared to these solutions.

Figure 8-2 shows the photograph of the solutions after they were allowed to sit for six hours without any disturbance. The picture shows that SWNT in water has completely settled down and in the case of Triton the tint was reduced compared to the previous picture. However, SDS and triton exhibited very stable suspensions with relatively high amount of SWNT suspended in the solution.

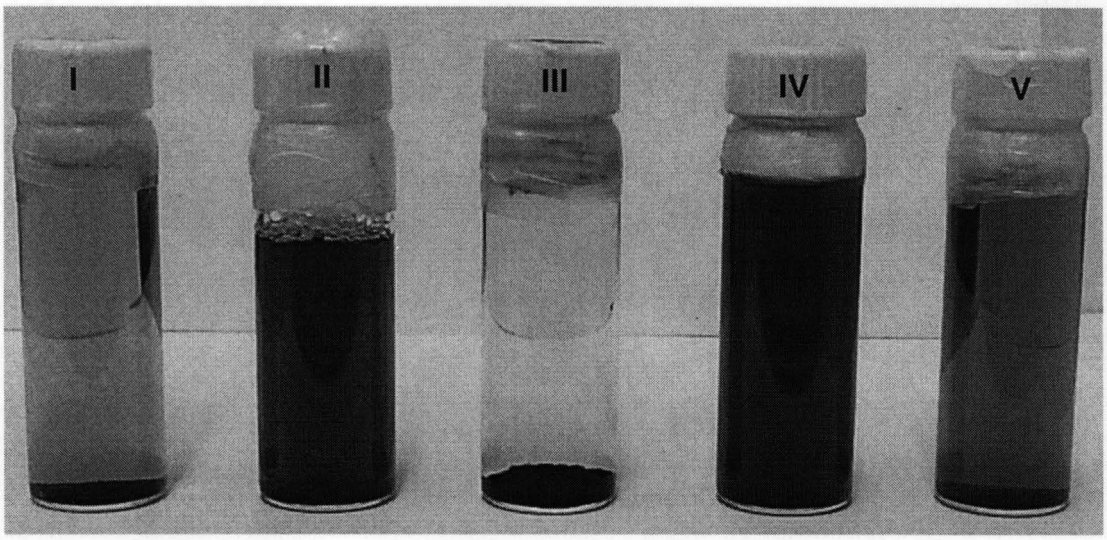

Figure 8-2. Solutions of various surfactants 6 hours after sonification (I) Triton-100 (II) SDS (III) DI water (IV) Tween 20 (V) IGEPAL CA 630.

In order to understand the mechanism behind this it is very important to know that CNT are highly hydrophobic in nature which is demonstrated by following experiment. Figure 8-3 shows the distribution of a 5µl water drop on the surface of silicon and CNT coated silicon.

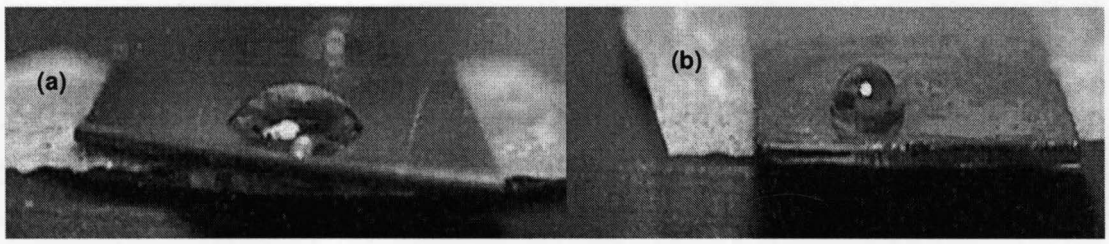

Figure 8-3. A 5µl water drop on (a) silicon (b) CNT coated silicon surface.

It can be clearly observed that the contact angle of water on CNT coated crystals was much higher compared to silicon which by itself is hydrophobic. This proves that CNT are higher hydrophobicity than silicon.

Previously many groups have studied the improved solubility of CNT on treating them with SDS. In order to understand this mechanism one should know that the CNT are highly hydrophobic in nature. SDS is like many typical surfactant molecules, in that it is composed of a hydrophilic `head' group, the charged sulphate group, and a hydrophobic `tail', the long hydrocarbon chain. The tail being hydrophobic interacts with the hydrophobic sidewalls of carbon nanotube. The chemisorptions of SDS molecules on the surface of the nanotubes form a distribution of negative charges that prevents their aggregation and induces stable suspensions in water.

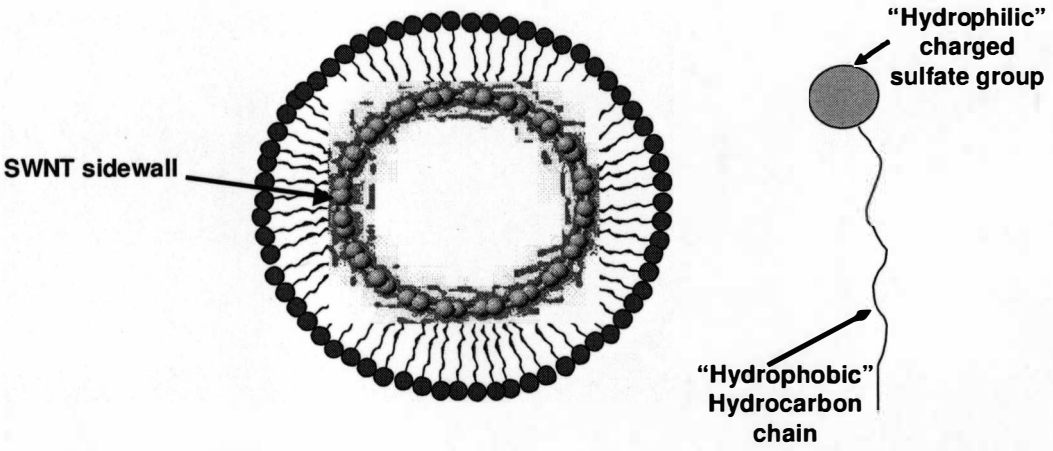

Figure 8-4. Cross-sectional view of SDS molecules adsorbing on SWNT side wall.

The SDS molecules can form different kinds of orientations on the surface of the nanotube [8]. The three possible orientations suggested in recent studies are

1. The SDS molecules may be adsorbed perpendicular to the surface of the nanotube, forming a monolayer.(as shown in Figure 8-4 and 8-5)
2. The SDS molecules may be organized into half cylinders oriented parallel to the tube axis.(as shown in figure 8-6)

3. The SDS molecules might form half-cylinders oriented perpendicular to the tube axis. .(as shown in figure 8-7)

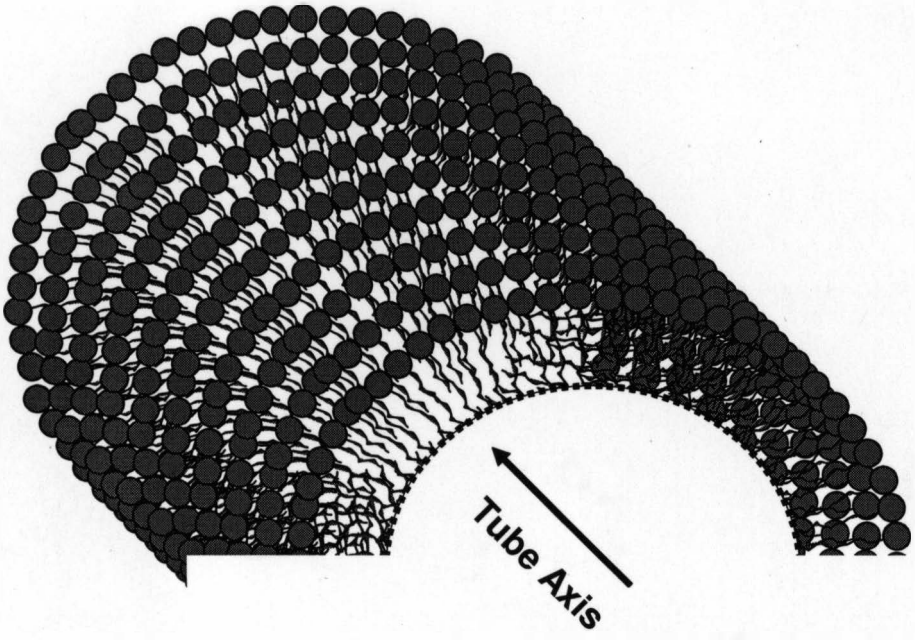

Figure 8-5. 3-Dimensional view of SDS molecules adsorbing on SWNT side wall.

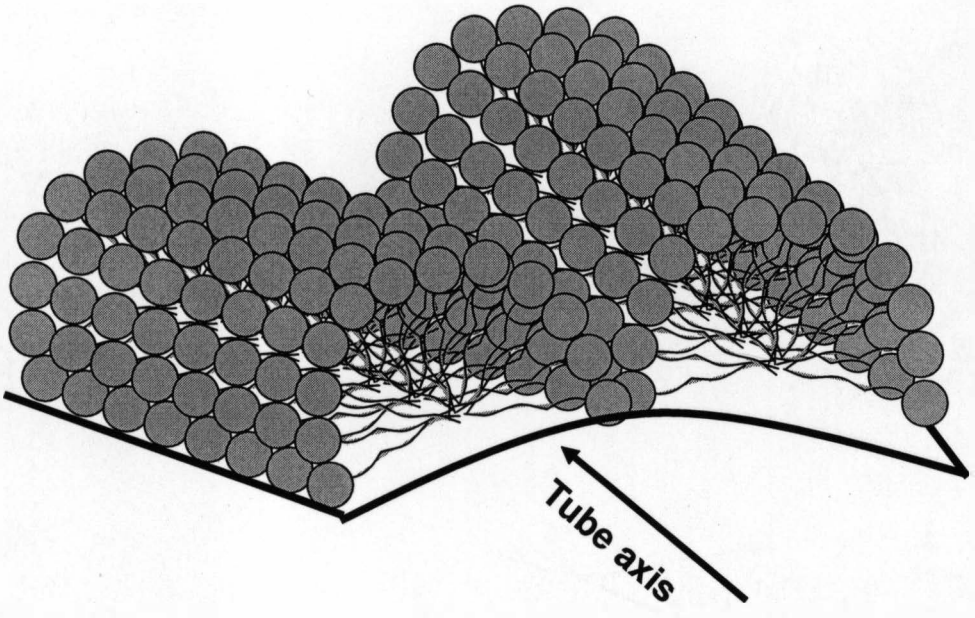

Figure 8-6. 3-Dimensional view of SDS molecules adsorbing on SWNT side wall as half cylinders parallel to axis of the tube.

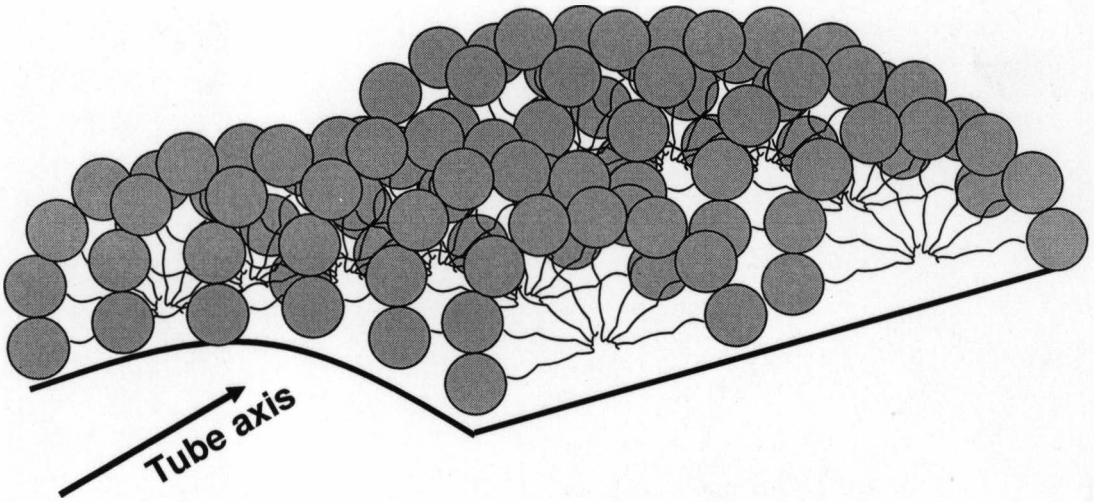

Figure 8-7. 3-Dimensional view of SDS molecules adsorbing on SWNT side wall as half cylinders perpendicular to axis of the tube.

The interesting aspect of the present study is that Tween 20 adsorption on CNT is comparable to that of SDS. This was verified in two ways. Firstly, the visual inspection of the CNT solution in Tween 20 shows a comparable black tint with SDS solution even after 2 days. This can be observed from the figure 8-8.

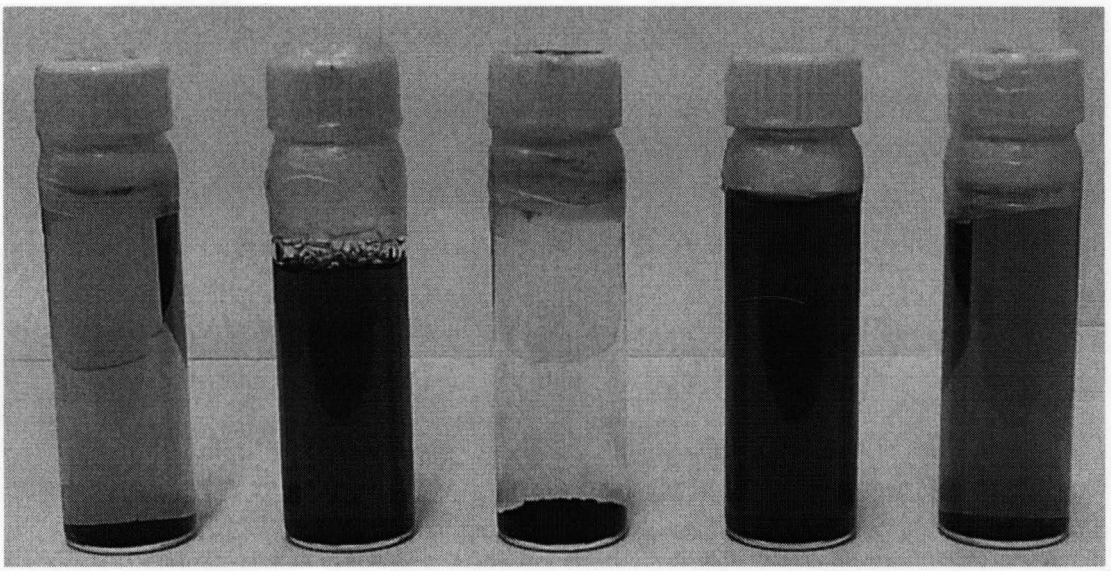

Figure 8-8. Solutions of various surfactants 2 days after sonification (I) Triton-100 (II) SDS (III) DI water (IV) Tween 20 (V) IGEPAL CA 630.

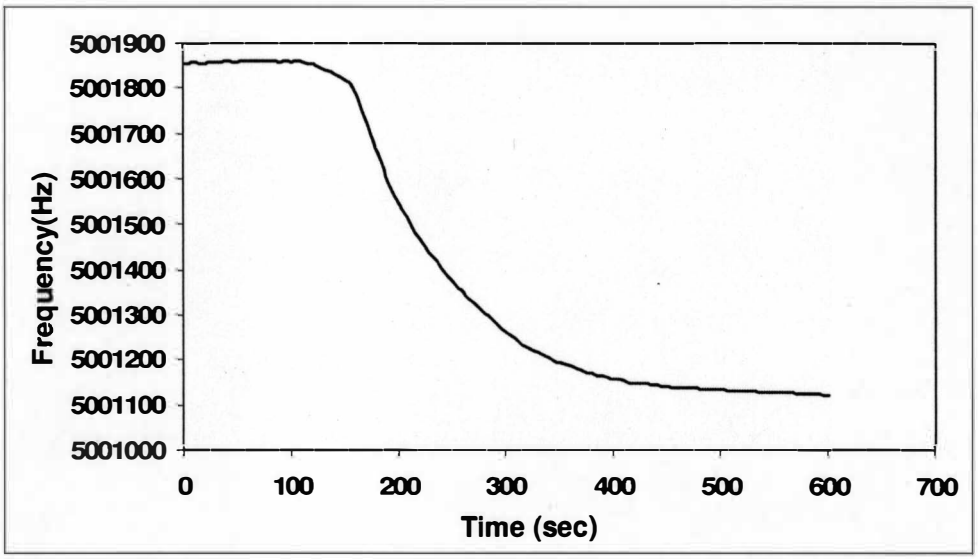

Figure 8-9. QCM response for 1% "Tween 20" on SWNT coated crystals.

In order to confirm this adsorption a QCM was employed. CNT coated crystals (as mentioned in chapter 7 section 4) were prepared and then the crystals were mounted in the holder. 200 µl of milli-Q water was placed on the chip.

After attaining a stable frequency 2 µl of Tween 20 was added to the chip. Figure 8-9 shows the QCM response of Tween 20 incubation on CNT surface. The change in the frequency of on QCM incubation was found to be ~730 Hz. This shows that Tween 20 also readily adsorbs on the sidewalls of SWNT. Similar experiments with IGEPAL showed that relatively high concentration of 4% was required for the same adsorption.

Figure 8-10 shows the QCM response to 4% IGEPAL CA-630.

The frequency shift for 4% of IGEPAL is ~515 Hz as opposed to the 730 Hz change in the case of 1% Tween 20. This lower frequency shift in the case of IGEPAL is in direct agreement with the visual observation of solutions shown in Figure 8-8. It can be seen

from the picture that the Tween 20 solution had a much darker tint compared to the IGEPAL solution. However Triton X-100 solution showed a poor dispersion of CNT and also a negligible response in the QCM experiment. This proves that Tween 20 had a comparable adsorption on CNT with that of SDS and the solution in both the cases were found to be stable for weeks. Although IGEPAL and TritonX-100 showed a poor dispersion, the former is slightly better compared to the later since it is slightly more hydrophobic. This causes it to have more hydrophobic-hydrophobic interaction with the CNT sidewalls.

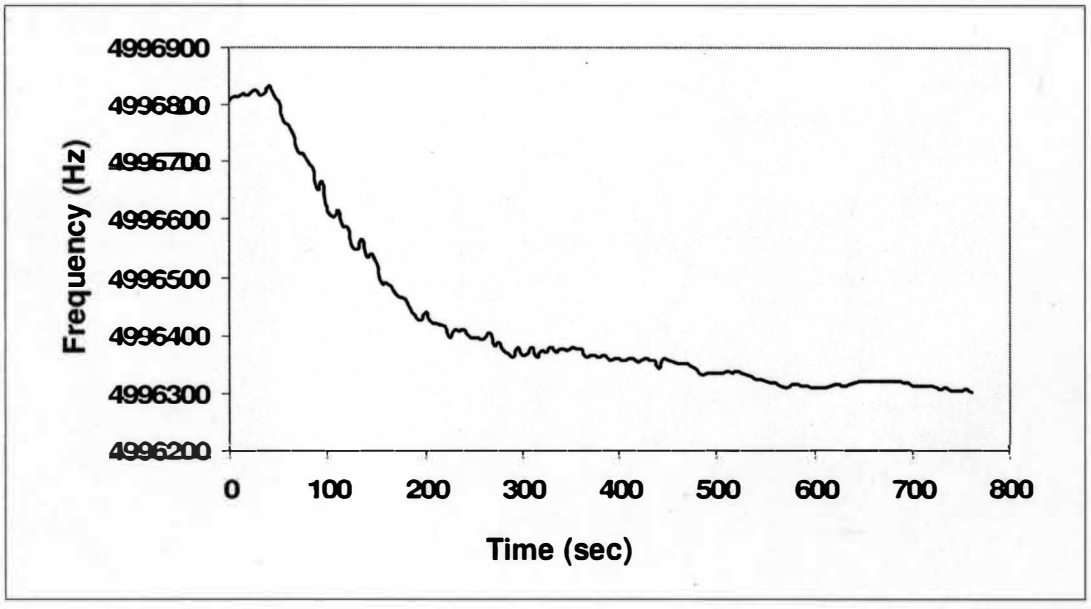

Figure 8-10. QCM response for 4% "IGEPAL CA-630" on SWNT coated crystals.

In conclusion we have found that SWNTs can be forced to dissolve in aqueous solution with the treatment of various surfactants. The common principle is that the surfactant molecules adsorb on the surface of the tube because of their amphiphilic nature. In

paticular hydrophobic part of these molecules is chemisorbed on the SWNT sidewalls. The molecules adsorbed on the surface reduce the Van der- waal forces between the nanotubes making them soluble in water media. This is a significant result in extending the biological sensing abilities of carbon nanotubes. Tween 20 is well known surfactant in the biology laboratories as a protein resistant. It will be interesting to study the protein resistance of carbon nanotubes modified with various surfactants. Thus the selectivity of carbon nanotubes based sensors can be improved with the treatment of various surfactants.

8.5. References

[1]. J. Chen, M. A. Hammond, M. Hui, C. Yongsheng, A. M. Rao, P. C. Eklund, and R. C. Haddon, Science, vol. 282, p. 95, (1998).

[2]. J. L. Stevens, A. Y. Huang, H. Peng, I. W. Chiang, V. N. Khabashesku, and J. L. Margrave, Nanoletters, vol.3, p.331, (2003).

[3]. J. Kong, M. G. Chaplin, and H. Dai, Advanced Materials, vol. 13, p. 1384, (2001).

[4]. R. J. Chen, Y. Zhang, D. Wang, and H. Dai, Journal of American Chemical Society, vol. 123, p.3838, (2001).

[5]. R. J. Chen, S. Bangsaruntip, K. A. Drouvalakis, N. W. Shikam, M. Shim, Y. Li, W. Kim, P. J. Utz and H. Dai, PNAS, vol. 100, p. 4984, (2003).

[6]. E.T. Thean, and B.H. Toh, Analytical Biochemistry, vol. 177, p. 256, (1989).

[7]. S. Lund et al., Journal of Biological Chemistry, vol. 264, p. 4907, (1989).

[8]. C. Richard, F. Balavoine, P. Schultz, T. W. Ebbesen, and C. Mioskowski, Science, vol. 300, p. 775, (2003).

9. CONCLUSIONS AND FUTURE WORK

9.1. Summary

The goal of the research was to investigate the potential application of carbon nanotubes as chemical and biological sensors at molecular level. Although this was the main goal some intriguing effects relating to the basic physics of carbon nanotubes which might significantly influence the main stream of the research were carefully studied. This research brings into light a novel and simple technique of obtaining high purity SWNT solutions. Obtaining highly pure SWNT matrices is significant achievement owing to the numerous studies and applications of CNT. Raman spectrum of SWNT exhibited a downward shift of the G-band peak at elevated temperatures. This was further explored by comparative studies of downward shift of G-band in SWNT and HOPG. The variation in their temperature dependence was explained with respect to their structural variation.

The biosensing applications proved that the nanotubes are potential choice in next generation of nano-biosensors. Biomolecules like Streptavidin and Mouse Monoclonal IgG readily adsorbed on the surface of the SWNT due to the hydrophobic interactions. This was studied and quantified by two types of sensors namely the conduction based sensors and the Quartz crystal microbalance. Some chemical sensing applications like NH_3 and NO_2 have been previously demonstrated. A new facet in the chemical sensing applications of SWNT was demonstrated by proving that the electronic properties of SWNT are sensitive to alcohol vapors.

Finally the functionalization of Carbon Nanotubes with various surfactants revealed an interesting fact that Tween 20 is also a good choice in addition to SDS for forming stable

aqueous solutions. This was also confirmed with QCM and reasons behind this behavior were discussed. This forms the first step towards the improvement of selectivity of biosensors based on carbon nanotubes.

The work presented in this thesis has resulted in two conference publications (IEEE sensors 2004, and MRS Fall meeting 2004) and a journal paper in under review (Applied Physics Letters).

9.2. Future work

There are many aspects which are very closely related to the main area of this work and could not be devoted enough time. A structural investigation is required to understand and relate the morphological changes of SWNT and the anomalous behavior observed in the Raman spectrum at elevated temperatures. The conduction based biological and chemical sensors demonstrated in this work are basically two electrode proto types. A three electrode model resembling a FET can be constructed and the influence of the gate voltage on the sensing properties can be studied. Theoretically the gate voltage should increase the sensing ability of the SWNT. The research can be continued in order to explore the possible ways of detecting serum proteins, including disease markers, autoantibodies, and antibodies. Further investigation regarding the biological sensing application for detection of specific biomolecules by functionalization of SWNT is suggested. Biological specificity, in conjunction with the exclusive electronic properties of nanotubes might enable nanotube-based biosensors to selectively detect proteins in solution by using direct electronic signaling obviating any need for complex circuitry or conventional radioactive labeling.